

**ROBOTIC CONTOUR TRACKING WITH FORCE CONTROL
AND AN OPERATIONAL SPACE DISTURBANCE OBSERVER**

by HAKKI BARAN ÖZDAMAR

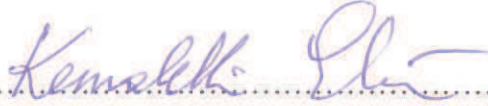
Submitted to the Graduate School of Engineering and Natural Sciences
in partial fulfillment of the requirements for the degree of Master of Science

Sabancı University
August 2016

ROBOTIC CONTOUR TRACKING WITH FORCE CONTROL AND
AN OPERATIONAL SPACE DISTURBANCE OBSERVER

APPROVED BY:

Assoc. Prof. Kemalettin Erbatur
(Thesis Supervisor)



Prof. Mustafa Ünel



Assoc. Prof. Zeki Yağız Bayraktaroğlu



DATE OF APPROVAL: 08.08.16

© Hakkı Baran Özdamar 2016

All Rights Reserved

ABSTRACT

ROBOTIC CONTOUR TRACKING WITH FORCE CONTROL AND AN OPERATIONAL SPACE DISTURBANCE OBSERVER

HAKKI BARAN ÖZDAMAR

Mechatronics Engineering, M.Sc. Thesis

Thesis Supervisor: Assoc. Prof. Kemalettin Erbatır

Keywords: contour tracking, force control, hybrid control, disturbance observer,
contact estimation

Robots in the industry are used for operations that are particularly dangerous or challenging to complete with high efficiency and precision for humans. These robots require extensive programming to achieve high level tasks and reprogramming to repeat the task in different environmental conditions. Introducing some level of autonomy for the robots is desired to decrease the burden on the programmer by enabling the robot to adapt to environmental changes and accomplish the required tasks with minimal human interaction. Contour tracking is a task that can be completed autonomously by a robot and assist in the completion of several industrial operations in the process such as grinding, deburring, polishing and shape recovery. Hybrid control is a popular method for achieving contour tracking. This thesis presents a hybrid controller that employs feedforward and integral force actions in the contact normal direction; and dynamics based proportional velocity control with disturbance estimation in the tangent direction. The effectiveness of the presented method has been validated and its superiority compared to conventional PI velocity control is proven experimentally. A simple and reliable method for contact estimation is also presented.

ÖZET

KUVVET KONTROLÜ VE OPERASYONEL UZAYDA BOZUCU ETMEN GÖZLEMCİSİ İLE ROBOTİK KONTUR İZLEME

HAKKI BARAN ÖZDAMAR

Mekatronik Mühendisliği, Master Tezi

Tez Danışmanı: Doç. Dr. Kemalettin Erbatur

Anahtar kelimeler: kontur izleme, kuvvet kontrolü, hibrit control
bozucu etmen gözlemcisi, temas kestirimi

Endüstrideki robotlar birçok tehlikeli, veya insanlar için yüksek verim ve kesinlik ile tamamlanması güç olan operasyonlarda kullanılır. Bu robotlar yüksek seviye görevleri yerine getirmek için kapsamlı programlanmaya ve farklı çevresel koşullarda görevleri tekrarlamak için yeniden programlanmaya ihtiyaç duyar. Robotun çevresel değişimlere adapte olabilmesini ve istenen görevleri asgari insan etkileşimi ile yerine getirebilmesini sağlayarak, robotu programlayanın üzerindeki yükün azaltılması amacıyla robotların otonomluğunun artırılması istenmektedir. Kontur izleme, robotun otonom bir şekilde tamamlayabileceği bir görev olup, aynı zamanda taşlama, çapak alma, parlatma ve şekil öğrenme gibi endüstriyel operasyonların tamamlanmasında yardımcı olabilir. Hibrit kontrol, kontur izleme uygulaması için sık kullanılan bir yöntemdir. Bu tez; temas normali yönünde kuvvet ileri besleme ve integral kuvvet kontrolü, temasa teğet yönde bozucu etmen gözlemcili dinamik bazlı oransal hız kontrolü kullanan bir hibrit kontrolör sunmaktadır. Sunulan kontrolün etkisi deneysel olarak onaylanmış ve konvensiyonel PI hız kontrolünden üstünlüğü kanıtlanmıştır. Ayrıca, basit ve güvenilir bir temas kestirim yöntemi sunulmaktadır.

ACKNOWLEDGEMENTS

I would like to express my gratitude to my advisor Assoc. Prof. Kemalettin Erbatur for giving me the freedom to work on and implement my own methods without withholding criticism. I am grateful to him for guiding me through the problems I have faced and helping me with tasks of the most trivial kind, as well as the more complex ones. He has been a mentor, not only on engineering but also on decency which is as valuable, if not more.

Besides my advisor, I would like to thank the thesis defense committee members: Prof. Mustafa Ünel and Assoc. Prof. Zeki Yağız Bayraktaroğlu. Their comments and critique on my work are deeply valued.

I would also like to express my gratitude to Professor Emeritus Asif Sabanovic for teaching all his students the value of our potential to learn and discover new ideas. His disposition in his classes and his advices outside have drove me to trust myself and to always strive to be better at whatever I do.

I am indebted to my friends and colleagues who shared the mechatronics research lab with me. Without them, the lab would be dull and the many hours spent in research and experimentation would be longer and much more boring.

Finally, I would like to thank my little brother for keeping my mind sharp with his endless, eccentric questions about my profession and engineering in general.

TABLE OF CONTENTS

1. INTRODUCTION	1
1.1. Contour Tracking	1
1.2. Problem Definition	3
1.3. Literature Review	4
1.4 Disturbance Observer	6
2. ROBOT MODEL AND CONTROL DESIGN	8
2.1 Robot Dynamics	9
2.2. Motion Control	11
2.2.1. Configuration Space Motion Control	11
2.2.2. Operational Space Motion Control	14
2.3. Force Control and Contour Tracking	15
2.3.1. Hybrid Velocity/Force Control	16
2.3.2. Determining the Contact Angle	19
3. EXPERIMENTAL SETUP, IMPLEMENTATION AND RESULTS	21
3.1. Experimental Setup	21
3.2. Implementation Issues	23
3.3. Experimentation and Results	25
3.3.1. The Effect of Cut-Off Frequency	25
3.3.2. The Effect of Disturbance Observer Gain/Bandwidth	27
3.3.3. The Effect of Contact Estimation Learning Parameter	29
3.3.4. Demonstration of the Contribution of Disturbance Observer	33

3.3.5. Increasing the Normal Force and Contour Tracking Velocity Commands.....	38
4. DISCUSSION AND CONCLUSION	43
4.1. Possible Improvements and Future Work	44
REFERENCES	45

LIST OF TABLES AND FIGURES

Figure 1.1: Sample of the contour of the workpiece used in the experiments.....	2
Figure 2.1: Experimental robot with the base coordinate frame and the generalized coordinates indicated.....	8
Figure 2.2: Experimental robot with the tool attached.....	9
Figure 2.3: Length parameters in the dynamics equation.....	10
Figure 2.4: CAD model of the robot showing the links.....	11
Figure 2.5: Contour coordinate frame.....	17
Figure 2.6: Overall block diagram of hybrid velocity/force controller.....	20
Table 3.1: Dynamics Parameters.....	22
Figure 3.1: Image of the workpiece showing entirety of its contour.....	23
Figure 3.2: Comparison of the filtered and raw joint angle measurements.....	24
Figure 3.3: Cut-off frequency comparison - control torques.....	26
Figure 3.4: Cut-off frequency comparison - tooltip velocity.....	27
Figure 3.5: Disturbance observer gain comparison- normal force tracking.....	28
Figure 3.6: Disturbance observer gain comparison - velocity tracking.....	28
Figure 3.7: Disturbance observer gain comparison - estimated contact normal.....	29
Figure 3.8: Learning parameter comparison – measured tangent force.....	30
Figure 3.9: Learning parameter comparison - velocity reference directions at the tip of the contour.....	31
Figure 3.10: Learning parameter comparison - estimated contact normal angles.....	32
Figure 3.11: Learning parameter comparison - velocity reference directions at the	

corner of the contour.....	32
Table 3.2: Control Parameters.....	34
Figure 3.12: Normal force response for conventional PI.....	35
Figure 3.13: Velocity response of conventional PI.....	35
Figure 3.14: P+DOB vs. dynamics based PI – force tracking.....	36
Figure 3.15: P+DOB vs. dynamics based PI - velocity tracking.....	36
Figure 3.16: Traversed path with P+DOB.....	37
Figure 3.17: Traversed path with dynamics based PI.....	37
Figure 3.18: 20 N normal force command - force tracking.....	39
Figure 3.19: 20 N normal force command - velocity tracking.....	39
Figure 3.20: 20 N normal force command - estimated tangent disturbance.....	40
Figure 3.21: 20 N normal force command - velocity vector directions at the corner.....	40
Figure 3.22: 20 mm/s contour tracking velocity command - force tracking.....	41
Figure 3.23: 20 mm/s contour tracking velocity command - velocity tracking.....	42
Figure 3.24: 20 mm/s contour tracking velocity command - traversed path.....	42

LIST OF SYMBOLS AND ABBREVIATIONS

PID	: Proportional integral derivative
DSP	: Digital signal processor
CAD	: Computer aided design
PI	: Proportional integral
DOB	: Disturbance observer
RMS	: Root mean square
q	: Joint angle vector
\dot{q}	: Joint velocity vector
\ddot{q}	: Joint acceleration vector
$D(q)$: Configuration space inertia matrix
$C(q, \dot{q})$: Matrix that contains the centrifugal and Coriolis terms affecting configuration space dynamics
$g(q)$: Configuration space gravity vector
τ	: Torque vector
τ_f	: Joint friction vector
$J(q)$: Jacobian matrix
F_{ext}	: External force vector
m_1	: Mass of link 1
m_2	: Mass of link 2
l_1	: Length of link 1
l_2	: Length of link 2

l_{c1}	: Distance from the joint to the center of mass for link 1
l_{c2}	: Distance from the joint to the center of mass for link 2
q_1	: First (shoulder) joint angle
q_2	: Second (elbow) joint angle
I_1	: Moment of inertia of link 1
I_2	: Moment of inertia of link 2
J_1	: Rotor inertia of motor 1 (shoulder motor)
J_2	: Rotor inertia of motor 2 (elbow motor)
\dot{q}_1	: First (shoulder) joint angular velocity
\dot{q}_2	: Second (elbow) joint angular velocity
\ddot{q}_{des}	: Desired joint acceleration vector
$\hat{\tau}_{dis}$: Estimated disturbance torque vector
D_n	: Nominal configuration space inertia matrix
τ_{dis}	: Disturbance torque vector
$\tilde{D}(q)$: Configuration space inertia matrix uncertainty
$\tilde{C}(q, \dot{q})$: Uncertainty of the matrix that contains the centrifugal and Coriolis terms affecting configuration space dynamics
g_{CS-DOB}	: Configuration space disturbance observer gain/bandwidth
e_q	: Joint angle error vector
q^{ref}	: Reference joint angle vector
K_D	: Derivative gain
K_P	: Proportional gain
K_I	: Integral gain

x	: Cartesian position vector
\dot{x}	: Cartesian velocity vector
\ddot{x}	: Cartesian acceleration vector
$\Lambda(q)$: Operational space inertia matrix
$\mu(q, \dot{q})$: Matrix that contains the centrifugal and Coriolis terms affecting operational space dynamics
$\gamma(q)$: Operational space gravity vector
F	: Tooltip force vector
\ddot{x}^{des}	: Desired Cartesian acceleration vector
e_x	: Cartesian position error vector
x^{ref}	: Reference Cartesian position vector
x_x	: x-coordinate of the Cartesian position
x_y	: y-coordinate of the Cartesian position
F^{dis}	: Disturbance force vector
θ_n	: Contact normal angle
$R_c(\theta_n)$: Rotation matrix that describes the contour coordinate frame
f^n	: Normal force
f^t	: Tangent force
f^{ref}	: Reference normal force
K_f	: Force feedback gain
F_m	: Force measurement vector
\hat{F}^{dis}	: Estimated disturbance force vector
e_v	: Velocity error vector

v^{ref}	: Reference velocity vector
K_v	: Velocity feedback gain
f_c	: Normal force command
v_c	: Contour tracking velocity command
g_{CT-DOB}	: Contour tracking disturbance observer gain/bandwidth
K_θ	: Contact estimation learning parameter
f_{bias}^t	: Bias force in tangent direction
f_x	: Force measurement in x-direction
f_y	: Force measurement in y-direction
u_1	: Control signal for motor 1 (shoulder motor)
u_2	: Control signal for motor 2 (elbow motor)
q_{filt}	: Filtered joint angle vector
g_q	: Cut-off frequency for joint angle filter
\hat{q}	: Estimated joint velocity vector
u_{PI}	: Control effort vector computed by PI scheme

Chapter 1

1. INTRODUCTION

The reason of the existence of robots is to ease the life of humans by taking over tasks of the dangerous, repetitive and banal kind. The reason for them becoming more and more popular in the industry, however, is also due to the fact that robots being far more reliable and successful in completing such tasks than humans, given they are properly designed and programmed. Despite that, robots are still quite behind humans when the task at hand requires a skill much more valuable than precision or repeatability: reasoning. One of the objectives in industrial robotics is to create robots that can employ some level of reasoning to realize a given high level task instead of following a series of low level commands written for them by a human, which may require tedious programming and take precious time. In other words, the aim is to create autonomous robots that can complete their tasks with minimum human interaction.

Contour tracking is a task that can be completed autonomously and assist in the completion of several dangerous and repetitive industrial operations in the process.

1.1. Contour Tracking

The contour refers to a two dimensional curve that binds an object. In the context of robotic manipulation, the contour would be defined by the edges of the workpiece, the object that is manipulated, or the cross-section of the workpiece by the plane on which the motion is constrained for contour tracking purposes. Autonomous tracking of the contour would enable a robot to achieve several tasks common in the industry without

human interaction or guidance; such as grinding, deburring, polishing and shape recovery. Automation of such tasks can be handled using robotic arms and conventional position control. However, reliable robotic operation and satisfactory results would require detailed knowledge of the workpiece shape, its location and pose. This requirement imposes the need for reprogramming the robots for each different workpiece and task; or in more advanced robotic systems, teaching the shape of the workpiece and the required task to the robot with the guidance of a human operator. These needs are eliminated with the realization of autonomous contour tracking, further decreasing the required labor force in industrial automation.



Figure 1.1: Sample of the contour of the workpiece used in the experiments

Apart from its assistance for aforementioned tasks, contour tracking can also be employed for motion planning in a cluttered and unstructured workspace. If the contact with obstacles in a workspace can be detected, contours of the detected obstacles can be tracked to generate alternative paths to desired configurations and to target points. Contact detection or contact sensing, meaning detecting the existence, location and direction of contact on the body of the robot is a problem associated with contour tracking. One of the most popular methods to detect contact at the tooltip is using force measurements from a force sensor attached at the wrist of the robot. However, given that the system dynamics is known and common internal disturbances such as friction is identified and modeled, sensorless contact detection is also possible using reaction force observer [1-2]. Moreover, contact force measurement is not the only method of feedback for the contour tracking task. Visual feedback and visual servoing based control have also been applied [3-4].

1.2. Problem Definition

The aim of this thesis is to develop control which will enable a manipulator to achieve autonomous contour tracking on objects of varying shapes. The main design concern is autonomy. Robot autonomy in the context of contour tracking means that the robot should be able to carry out the contour tracking task without knowing the shape, location or pose of the workpiece beforehand. A given motion command to the vicinity of the workpiece that guarantees contact would be the only human interaction with the robot. The developed control should also be robust, such that the contour tracking task should be achievable on workpieces with rough or deformed edges with occasional discontinuities. The autonomy of the robot can be further extended by leaving the task of reaching the workpiece to the robot as well. Visual information of the workspace can be used to identify the workpiece and roughly determine its position, or the robot can simply be tasked to search for the workpiece inside its workspace. However, the task of autonomously finding the workpiece have not been considered as part of this thesis.

Further problems arise as high disturbances during control of robot for the contour tracking task. The frictional forces at the contact are unpredictable and would differ for each workpiece, robot tool and operation during contour tracking. Friction at the joints

is another disturbance as it is difficult to model and have a consistent estimate of the effect of friction on robot motion. Such disturbances should be compensated in order to accomplish precise motion and successful contour tracking.

1.3. Literature Review

Contour tracking as a means for shape recovery has been discussed in the paper by Ahmad and Lee [5]. The algorithm they present for the shape recovery problem is a step by step motion along the contour; meaning a predefined position step will be taken, contact direction will be computed provided the contact is kept and a new point on the contour will be defined. The determination of contact direction is based on the joint stiffness matrix of the robot and the force measurements.

The hybrid control method is proposed by Raibert and Craig [6] as control for situations where the manipulator position is needed to be controlled in a certain direction and force is needed to be controlled in a different direction independently. Therefore, hybrid control is suitable as control for the contour tracking task.

A control approach similar to the one taken in this thesis for contour tracking has been presented by Yoshikawa and Sudou [7] more than two decades ago. They have called it dynamic hybrid position/force control as the controller tries to compensate for robot dynamics. The proposed method relies on accurate calculation of robot dynamics, including estimation of a viscous friction matrix, as it does not include an integral term to compensate against model inaccuracy. An estimator for the contour tangent using force measurements and tooltip position data have been presented. They report satisfactory tracking performance of a smooth unknown contour described by a planar cross-section of a stainless steel bowl.

Another hybrid position/force control is mentioned by Bossert et al. [8] for the contour tracking task in which higher order controllers are applied. The tracking mechanism is a low friction roller which virtually only senses the normal contact force, hence the contour direction can be inferred directly from the force measurements. A similar situation does exist for the experimental setup used in this thesis as well, where the contact with the contour is established by the head of the grinding tool attached to the

robot which is a rolling mechanism and therefore would not sense significant tangent force. However, static friction at contact and viscous friction still remains as disturbance.

Whitcomb et al. presents research on adaptive model based hybrid control for motion constrained in a plane described by the surface of a smooth object [9]. This approach is applicable for contour tracking as well. They present a sliding-mode based hybrid position/force controller. The paper, however, is not concerned with automatic detection of the surface gradient and assumes that the position reference is known beforehand.

More recent research on contour tracking by Jatta et al. [10-11] employs hybrid velocity/force control instead of position/force control. Their proposed method is not model based, but simple feedforward and feedback schemes using velocity reference and feedback for tangent direction and force reference and feedback in normal direction. They present a unique friction compensation method which involves modeling of friction as a polynomial function of joint velocities. Two methods for approximating such a polynomial have been presented: static and adaptive. While static method uses simple offline estimation based on least squares algorithm with experimental data at hand to obtain the parameters of the aforementioned polynomial; the adaptive method shows development of a neural network to enable the robot to learn the said parameters online. It is shown that adaptive friction compensation outperforms the static method experimentally. Since the friction model is generated according to the joint velocities, the friction compensation method is valid for viscous friction but cannot compensate for friction at contact or static friction at robot joints. The detection of contour direction is done by using solely force measurements which is feasible for the experiments presented where the contact exhibits low dynamic friction and the contour is not varying.

A study done by Mi and Jia [12] employs a high precision commercial robot as the experimental manipulator and uses hybrid position/force controller as the control for the contour tracking task. The unreliability of using solely force measurement in constructing the contour trajectory have also been addressed in their study. They define the estimated tangential angle as a function of the arc length between each position reference on the contour, and they approximate the arc length as the distance between said position references; which is feasible if the steps taken as position reference is

small and the contour does not exhibit sharp discontinuities. The presented method for contact direction detection predicts the future tangent angles using the previous ones and updates the estimated angle using both the predicted angle and the measured force data. They report precise estimation and tracking of curved contours.

1.4. Disturbance Observer

A model based hybrid velocity/force controller has been used as the control for the contour tracking task in this thesis. Furthermore, the motion controllers implemented are model based as well. In order to compensate for model inaccuracies, non-modeled friction and other disturbances mentioned in section 1.2; utilization of disturbance observers is proposed. The design of the implemented disturbance observers is presented and explained in chapter two, however, a brief discussion about the advantages and the limitations of using disturbance observers as compensation will be presented here.

Robotic systems are highly non-linear systems. Control of such systems using conventional methods like PID requires extensive tuning for satisfactory performance. A way to decrease the burden on feedback control is to identify and feedforward the system dynamics. Although theoretical tools for obtaining the closed-form dynamics of electromechanical systems like robots is available as the Euler-Lagrange approach, accurate identification of dynamics parameters and application of theory on high complexity, higher degree of freedom systems is a challenge. Additionally, there are forces acting on the system that are difficult to model such as plant friction; and there may be external forces that simply cannot be predicted. Disturbance observers can be used to compensate for imperfect modeling, dynamics that cannot be modeled and external disturbances.

The disturbance observer is presented by Ohnishi et al [13] as a compensation tool for advanced mechatronic systems. Disturbance observers work based on a model that relates the control input to some system response. In the context of robotics, the dynamics equation (2.1) which presents a relation between the control torque/force vector and the dynamical motion response of the robot. If the motion response to a given control input is not in line with the model, that is assumed to be a result of

existence of some disturbance. That disturbance is observed and estimated by the disturbance observer which then fed back to the system, effectively forcing the system to mimic the model.

Implementation of disturbance observers are realized with the utilization of low-pass filters. Design considerations and limitations of the low-pass filters include the nature of disturbance [16], dynamics model parameter uncertainties [14], the noise associated with the measurement of motion response [15], and the control cycle time. Common problems using disturbance observer based compensation are chattering of the control signals due to noise in measurement, and ensuring stability. Disturbance observer gain or bandwidth is crucial for the performance and robustness of the system, but usually limited due to such problems in practice.

Chapter 2

2. ROBOT MODEL AND CONTROL DESIGN

This chapter presents the considered robot dynamics, describes the designed motion controllers tasked to realize configuration space and operational space motion commands. It also describes the simultaneous force control and contour tracking algorithm which is activated when the robot tooltip comes into contact with an unknown object.

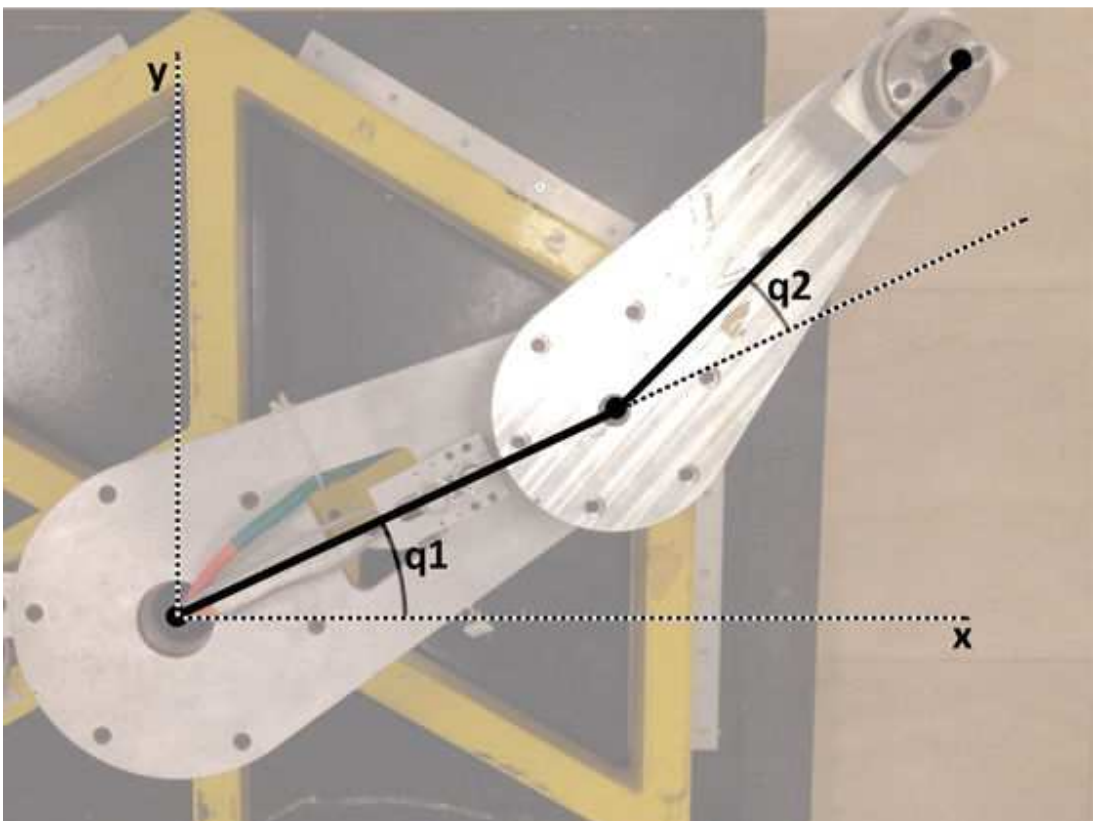


Figure 2.1: Experimental robot with the base coordinate frame and the generalized coordinates indicated

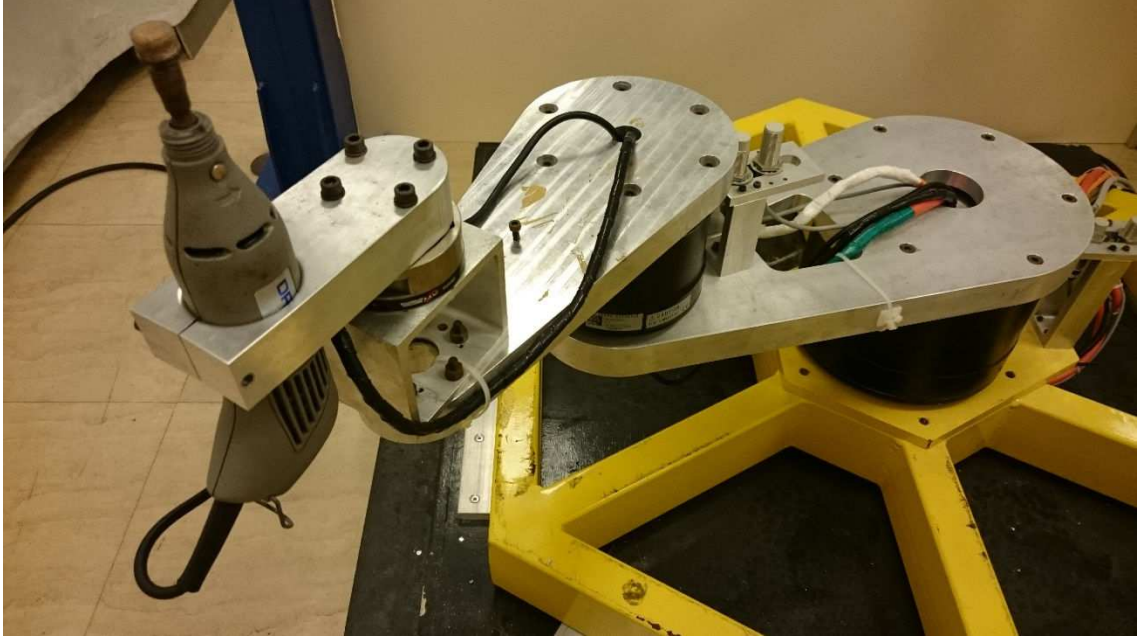


Figure 2.2: Experimental robot with the tool attached

2.1. Robot Dynamics

Robotic systems, in general, can be described by the following dynamics equation;

$$D(q)\ddot{q} + C(q, \dot{q})\dot{q} + g(q) = \tau \quad (2.1)$$

In the dynamics equation 2.1; $D(q)$ is the inertia matrix, $C(q, \dot{q})$ contains the centrifugal and Coriolis terms affecting the robot dynamics, $g(q)$ is the gravity vector and τ is the vector of joint torques. Gravity has no effect on the dynamics for the particular experimental robot (Fig. 2.1 and 2.2) used for this thesis since the gravitational acceleration lies on the same axis as joint axes and the links are not flexible. Hence, the gravity vector disappears from the dynamics equation. Considering the joint friction and external forces applied on the robot, 2.1 can be rewritten as;

$$D(q)\ddot{q} + C(q, \dot{q})\dot{q} + \tau_f + J(q)^T F_{ext} = \tau \quad (2.2)$$

Joint friction τ_f is a combination of static, kinematic and viscous friction. It is difficult to model and will be regarded as immeasurable disturbance for the remainder of this thesis.

The configuration of the experimental robot is exactly the same as the common configuration known in the literature as planar elbow manipulator. The dynamics matrices of a planar elbow manipulator, with the inclusion of motor dynamics, are given as [17];

$$D(q) = \begin{bmatrix} m_1 l_{c1}^2 + m_2(l_1^2 + l_{c2}^2 + 2l_1 l_{c2} \cos q_2) + I_1 + I_2 + J_1 & m_2(l_{c2}^2 + l_1 l_{c2} \cos q_2) + I_2 \\ m_2(l_{c2}^2 + l_1 l_{c2} \cos q_2) + I_2 & m_2 l_{c2}^2 + I_2 + J_2 \end{bmatrix} \quad (2.3)$$

$$C(q, \dot{q}) = \begin{bmatrix} -m_2 l_1 l_{c2} \sin q_2 \dot{q}_2 & -m_2 l_1 l_{c2} \sin q_2 (\dot{q}_1 + \dot{q}_2) \\ m_2 l_1 l_{c2} \sin q_2 \dot{q}_1 & 0 \end{bmatrix} \quad (2.4)$$

In 2.3 and 2.4; $m_{1,2}$ are the link masses, $l_{1,2}$ are the link lengths, $l_{c1,c2}$ denote the distance between the joint center and the center of mass of each link, $I_{1,2}$ are the moments of inertia for each link and $J_{1,2}$ are the rotor inertias.

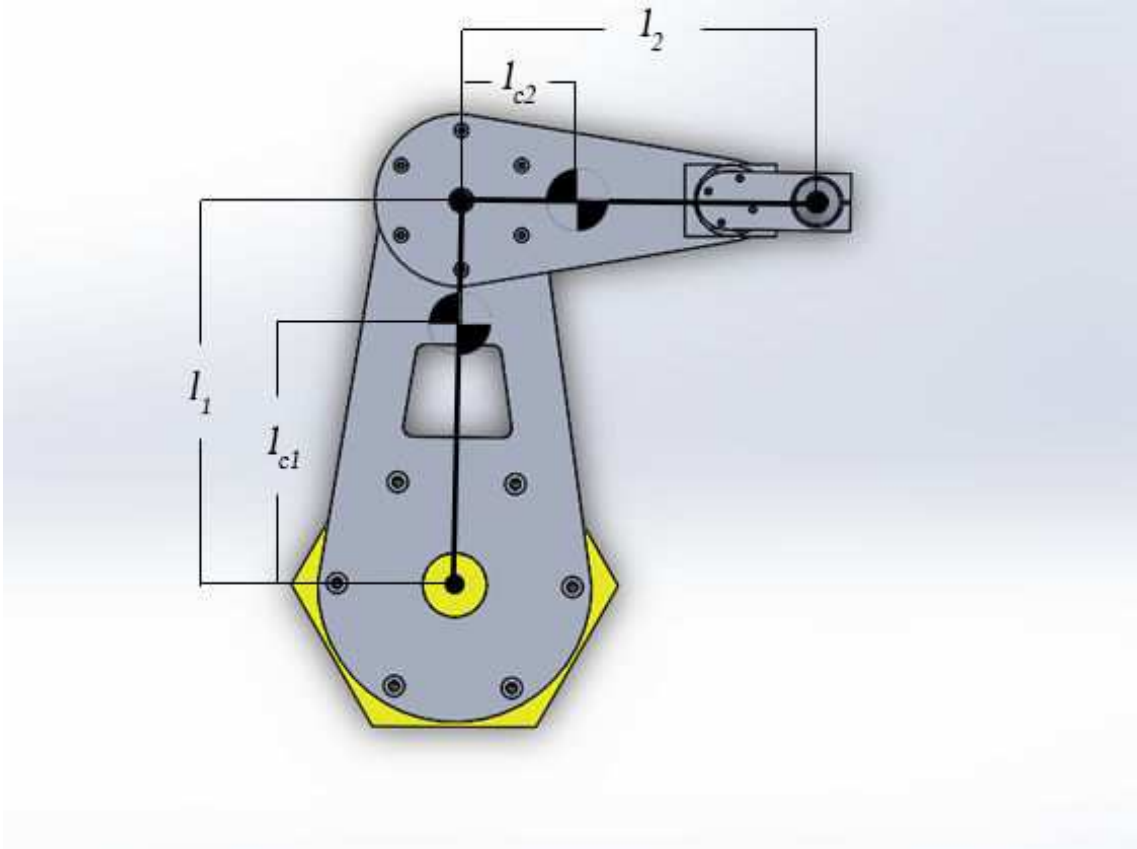


Figure 2.3: Length parameters in the dynamics equation

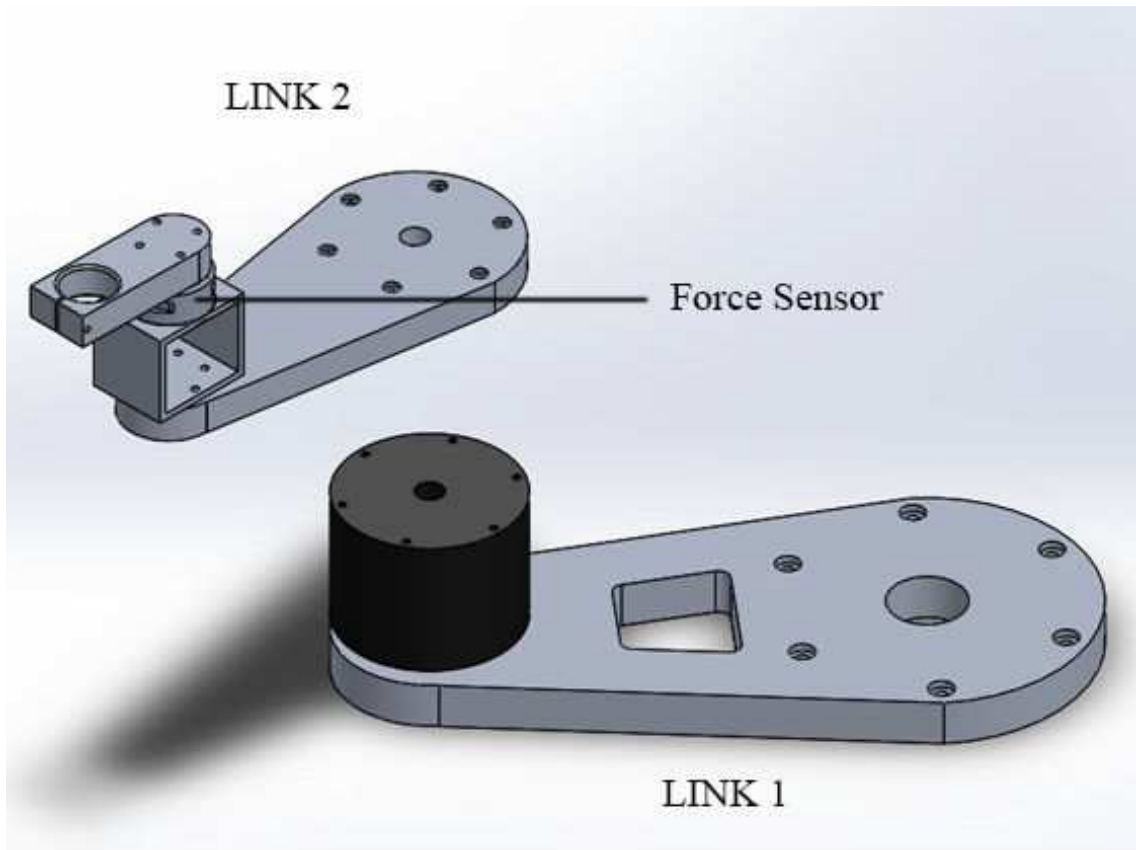


Figure 2.4: CAD model of the robot showing the links

2.2. Motion Control

Although this thesis is mainly concerned with force control and contour tracking, reasonable precision motion control is needed and desired to have the robot tooltip reach the workpiece. Both motion in configuration space and motion in operational space have been considered as part of the thesis work. Controllers for both types of motion have been designed and implemented. Trapezoidal/triangular trajectory generation method has been applied for all motion tasks.

2.2.1. Configuration Space Motion Control

Configuration or joint space motion is used to have the robot assume a desired configuration before moving towards the workpiece. This type of motion would be used when the robot is not expected to contact the workpiece or face an obstacle between the

initial and the desired configurations. In other words, when the traversed path in Cartesian space is unimportant. The objective in this motion is to attain steady state precision with high velocities. Inverse dynamics with disturbance observer has been employed as the method of control to achieve this objective.

$$\tau = D(q)\ddot{q}_{des} + C(q, \dot{q})\dot{q} + \hat{\tau}_{dis} \quad (2.5)$$

Implementation of the selected control input (2.5) requires closed-form dynamics matrices and updating their values in real-time, or online numerical computation of these matrices. This implementation is feasible for the experimental robot since closed-form matrices are already known and given in equations (2.3) and (2.4). Moreover, as they are 2x2 matrices, updating them does not take much computational effort and can easily be done in real-time. For higher degree of freedom and more complex robotic systems, selecting the control input as in (2.6) may be a better choice where the robot dynamics are regarded as disturbance.

$$\tau = D_n\ddot{q}_{des} + \hat{\tau}_{dis} \quad (2.6)$$

Selection of control input (2.5) implies that the considered disturbance is;

$$\tau_{dis} = \tilde{D}(q)\ddot{q} + \tilde{C}(q, \dot{q})\dot{q} + \tau_f + J(q)^T F_{ext} \quad (2.7)$$

In 2.7; $\tilde{D}(q)$ and $\tilde{C}(q, \dot{q})$ denote the inaccuracies between the modelled and actual robot dynamics. Most of the values used in calculation of the dynamics matrices are not exactly known but approximations, thus significant model inaccuracy is expected.

Rewriting (2.2) as;

$$\tau_{dis} = \tau - D(q)\ddot{q} - C(q, \dot{q})\dot{q} \quad (2.8)$$

(2.8) shows the direct calculation of the disturbance which is seldom possible because of the existence of \ddot{q} in the equation. Joint accelerations are rarely measurable and calculating them from motor encoder readings is very impractical due to associated noise. However, the need for explicit information of \ddot{q} is removed with the help of a low-pass filter.

$$\hat{\tau}_{dis} = (\tau - D(q)\ddot{q} - C(q, \dot{q})\dot{q}) \frac{g_{CS-DOB}}{s + g_{CS-DOB}} \quad (2.9)$$

$$\hat{\tau}_{dis} = (\tau + D(q)g_{CS-DOB}\dot{q} - C(q, \dot{q})\dot{q}) \frac{g_{CS-DOB}}{s + g_{CS-DOB}} - D(q)g_{CS-DOB}\dot{q} \quad (2.10)$$

Equations (2.9) and (2.10) are mathematically equivalent and it is shown that the joint acceleration vector is removed from the estimated disturbance equation. It is also possible to remove the joint velocity vector \dot{q} by utilizing a second order low-pass filter but it was not deemed necessary since it is possible to calculate it with relatively less effect from encoder noise; and explicit \dot{q} calculation is required to apply the position and velocity control laws presented in this thesis anyhow. Moreover, it is known that higher order low-pass filter based disturbance observer, while increasing the system performance, decreases control robustness [15].

In (2.9) and (2.10), g_{CS-DOB} is the configuration space disturbance observer gain which determines the cut-off frequency of the used low-pass filter, hence determining the associated time delay with it. Increasing the gain decreases the response time of the disturbance observer, thus enhancing its performance. From a frequency domain perspective; higher gain increases the disturbance observer bandwidth, enabling it to compensate for disturbances in wider frequency range. However, the disturbance observer gain is theoretically limited by control cycle time; it is also limited in practice by system robustness, measurement resolution and noise [13,15].

Error convergence to zero is enforced by selecting the appropriate \ddot{q}_{des} . The only measured state of the system is joint angles. Therefore, let us define the control error in terms of q as;

$$e_q = q^{ref} - q \quad (2.11)$$

Satisfying equations (2.12) and (2.13) would enforce exponential error convergence to zero if internal dynamics and disturbance is accurately estimated and fed to the system.

$$\dot{e}_q + K_1 e_q = \sigma_q \quad (2.12)$$

$$\dot{\sigma}_q + K_2 \sigma_q = 0 \quad (2.13)$$

Combining (2.12) and (2.13), and simplifying;

$$\ddot{q}_{ref} - \ddot{q} + K_D \dot{e}_q + K_P e_q = 0 \quad (2.14)$$

$$\ddot{q}_{des} = \ddot{q}_{ref} + K_D \dot{e}_q + K_P e_q \quad (2.15)$$

2.2.2. Operational Space Motion Control

Operational or task space motion is used to move the robot towards the workpiece with slow velocities in order to keep the impact force low. Moving towards the workpiece means traversing a linear path in Cartesian space from the initial tooltip position to somewhere behind, inside or on the edge of the workpiece. Detailed position information of the workpiece is not needed since the force control and contour tracking algorithm will be activated once the contact is established. Such a motion could also be achieved by using the configuration space motion control described in section 2.1.1. and utilizing inverse kinematics on a linear trajectory generated in Cartesian space. Since steady state precision is not important as the motion target would never be reached due to contact with the workpiece, disturbance observer or integral control is not needed. Regular inverse dynamics has been employed as control for operational space motion.

Operational space robot dynamics can be described by the following equations;

$$\Lambda(q)[\ddot{x} + \mu(q, \dot{q})\dot{q} + \gamma(q)] = F \quad (2.16)$$

$$\Lambda(q) = (J(q)D(q)^{-1}J(q)^T)^{-1} \quad (2.17)$$

$$\mu(q, \dot{q}) = J(q)D(q)^{-1}C(q, \dot{q}) - \dot{J}(q) \quad (2.18)$$

$$\gamma(q) = J(q)D(q)^{-1}g(q) \quad (2.19)$$

In (2.16), $\Lambda(q)$ is the operational space inertia matrix, $\mu(q, \dot{q})$ contains the terms related to centrifugal and Coriolis forces in operational space, $\gamma(q)$ is the operational space gravity vector and F is the force generated at the tooltip. Since gravity vector does not appear in the experimental robot's dynamics, the operational space gravity vector $\gamma(q)$ would not appear in the operational space dynamics. Then, (2.16) can be rewritten as;

$$\Lambda(q)[\ddot{x} + \mu(q, \dot{q})\dot{q}] = F \quad (2.20)$$

The relationship between joint torques and tooltip force is given as;

$$\tau = J(q)^T F \quad (2.21)$$

According to (2.20) and (2.21), inverse dynamics control input is selected as;

$$\tau = J(q)^T \Lambda(q)[\ddot{x}^{des} + \mu(q, \dot{q})\dot{q}] \quad (2.22)$$

Let us define tooltip position error as;

$$e_x = x^{ref} - x \quad (2.23)$$

Satisfying equations (2.24) and (2.25) would enforce exponential error convergence to a non-zero constant since there exists non-zero disturbance in the system, but this is sufficient for the objective of operational space motion control if the steady state system disturbance, which mostly corresponds to static friction, is small enough.

$$\dot{e}_x + K_1 e_x = \sigma_x \quad (2.24)$$

$$\dot{\sigma}_x + K_2 \sigma_x = 0 \quad (2.25)$$

Combining (2.24) and (2.25), and simplifying;

$$\ddot{x}^{ref} - \ddot{x} + K_D \dot{e}_x + K_P e_x \quad (2.26)$$

$$\ddot{x}^{des} = \ddot{x}^{ref} + K_D \dot{e}_x + K_P e_x \quad (2.27)$$

The tooltip position $x = [x_x \quad x_y]^T$ is computed via forward kinematics;

$$x_x = l_1 \cos(q_1) + l_2 \cos(q_1 + q_2) \quad (2.28)$$

$$x_y = l_1 \sin(q_1) + l_2 \sin(q_1 + q_2) \quad (2.29)$$

The tooltip velocity \dot{x} is computed as;

$$\dot{x} = J(q)\dot{q} \quad (2.30)$$

The Jacobian $J(q)$ is given as;

$$J(q) = \begin{bmatrix} -l_1 \sin(q_2) - l_2 \sin(q_1 + q_2) & -l_2 \sin(q_1 + q_2) \\ l_1 \cos(q_1) + l_2 \cos(q_1 + q_2) & l_2 \cos(q_1 + q_2) \end{bmatrix} \quad (2.31)$$

2.3. Force Control and Contour Tracking

The objective of the force control and contour tracking algorithm is twofold. First is to have the robot tooltip apply the desired amount of force perpendicular to the workpiece surface. Second is to have the robot tooltip track the contour, which is described by the edges of the workpiece, with desired velocity. These tasks are needed to be carried out simultaneously. Additionally, a background task of estimating the contour direction is necessary to guide the robot along the contour.

2.3.1. Hybrid Velocity/Force Control

Contour tracking requires slow and steady motion along the contour. Thus, centrifugal and Coriolis forces would be negligible when compared to contact forces and for simplicity, the operational space dynamics (2.20) can be reduced to;

$$\Lambda(q)\ddot{x} = F - F^{dis} \quad (2.32)$$

Neglecting $\mu(q, \dot{q})$ is reasonable because each element of it has a multiplicative factor of joint velocities \dot{q}_1 or \dot{q}_2 or their sum; and it is further multiplied by \dot{q} in the dynamics equation, resulting in very small effect in robot dynamics. (2.32) also introduces the disturbance force term F^{dis} . The assumed robot dynamics implies that; inaccuracy of the operational space matrix, neglected robot dynamics, contact forces and other plant disturbances such as joint friction are all considered as disturbance forces. Contact forces can be measured by the force sensor attached at the wrist of the robot but it is not possible to exactly determine the contribution of contact friction to these measurements. Therefore, it is convenient to regard all contact force as disturbance for the contour tracking task.

Let $R_c(\theta_n)$ be the rotation matrix that describes the contour coordinate frame as shown in Fig. 2.5. Translation of the frame is omitted.

$$R_c(\theta_n) = \begin{bmatrix} \cos(\theta_n) & -\sin(\theta_n) \\ \sin(\theta_n) & \cos(\theta_n) \end{bmatrix} \quad (2.33)$$

(2.32) can be rewritten using (2.33), showing the forces generated at the contact as follows;

$$\Lambda(q)\ddot{x} = R_c(\theta_n)[f^n \quad f^t]^T \quad (2.24)$$

In (2.24), f^n refers to the normal force and f^t refers to the tangent force generated at the contact according to the contour. The normal force would be selected in order to exert the required amount of force to the surface while the tangent force would be selected to enforce contour tracking with a desired velocity profile.

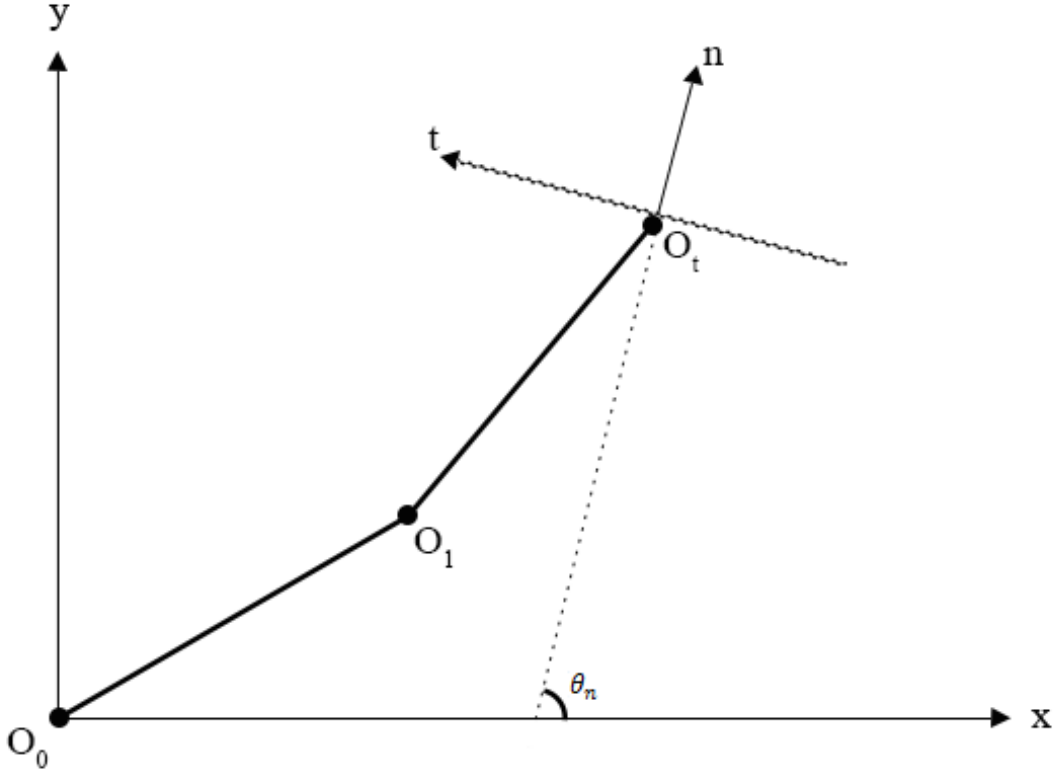


Figure 2.5: Contour coordinate frame

For an ideal plant without any disturbance, simply selecting f^n equal to the reference force f^{ref} would suffice, but mostly due to joint friction and also due to imperfect motor drives, feedforwarding the reference force alone would not be adequate. Force feedback control as compensator is needed. Therefore, the normal force command is selected as;

$$f^n = f^{ref} + K_f \int (f^{ref} - [1 \ 0]R_c(\theta_n)^T F_m) dt \quad (2.35)$$

Disturbance observer as designed for motion control is not appropriate to use as compensator for force error. Disturbance observer is model based and it works well with motion control because the considered dynamics equations define the relationship between the control input and associated motion. In order to be able to estimate disturbances during the generation of contact forces, a model to predict the contact forces with respect to control input is needed. This thesis is not concerned with developing such a model. On the other hand, integral control with force feedback is stable and effective in force tracking. Integral control guarantees zero steady state error

for a constant force reference and the lag associated with the controller prevents oscillations when the error changes rapidly.

Contour tracking is essentially a task of motion control. The same method of inverse dynamics used to develop operation space motion controller described in section 2.2.2. is adopted again for selection of the tangent force command;

$$f^t = [0 \quad 1]R_c(\theta_n)^T(\Lambda(q)\ddot{x}^{des} + \hat{F}^{dis}) \quad (2.36)$$

\ddot{x}^{des} can be selected as position feedback control or velocity feedback control. Precise position control in low velocities is not feasible in a direct drive robot as the experimental manipulator. The generated joint torques must first exceed the static friction at the joints in order to start motion which requires very high controller gains for low velocity motion, which in turn leads to overshoot and oscillations. This problem can be overcome for motion in free space if the consecutive coordinates of the motion trajectory is given as reference to the motion controller without waiting for the robot to reach the previous reference. That way, control effort will add up and eventually exceed the joint static friction. However, in contrast to motion in free space; during contour tracking, motion trajectory cannot be known beforehand, it is estimated at every step of the algorithm and extrapolation of the estimated trajectory to enforce motion would result in tracking error and it may also push the robot out from the contour or even in it if the workpiece has low stiffness. Therefore, velocity feedback control is a better choice for the contour tracking task. Defining velocity error as;

$$e_v = v^{ref} - \dot{x} \quad (2.37)$$

In (2.37), the velocity reference v^{ref} denotes the contour tracking velocity command rotated to be tangent to the contour.

$$v^{ref} = R_c(\theta_n)[0 \quad v_c]^T \quad (2.38)$$

Satisfying (2.39) would enforce error convergence to zero if the disturbance is accurately estimated and fed back to the system.

$$\dot{e}_v + K e_v = 0 \quad (2.39)$$

$$\dot{v}^{ref} - \ddot{x} + K_v e_v = 0 \quad (2.40)$$

$$\ddot{x}^{des} = \dot{v}^{ref} + K_v e_v \quad (2.41)$$

During the contour tracking task, motion is constrained by the workpiece. This constraint has not been introduced to the dynamics equation (2.32), thus it must be taken into account during the design of the disturbance observer for contour tracking. The disturbance observer must be blind to the applied normal force command f^n , otherwise it would compensate for the normal force generated at contact and try to force the robot through the contour. Then, the disturbance to be observed becomes;

$$F^{dis} = R_c(\theta_n)[0 \quad f^t]^T - \Lambda(q)\ddot{x} \quad (2.42)$$

Tooltip acceleration \ddot{x} information is not available. Thus, again a low-pass filter is utilized as done during configuration space disturbance observer design.

$$\hat{F}^{dis} = (R_c(\theta_n)[0 \quad f^t]^T - \Lambda(q)\dot{x}) \frac{g_{CT-DOB}}{s + g_{CT-DOB}} \quad (2.43)$$

$$\hat{F}^{dis} = (R_c(\theta_n)[0 \quad f^t]^T + \Lambda(q)g_{CT-DOB}\dot{x}) \frac{g_{CT-DOB}}{s + g_{CT-DOB}} - \Lambda(q)g_{CT-DOB}\dot{x} \quad (2.44)$$

Equations (2.43) and (2.44) are mathematically equivalent and they show that tooltip velocity \dot{x} which is obtained in (2.30) and contour normal angle θ_n are necessary and sufficient to realize contour tracking disturbance observer. Online computation of the operational space inertia matrix also requires the joint angle vector q . However, as mentioned in section 2.2.1, disturbance observer can also be designed by selection of a nominal inertia matrix with constant elements. In that case, the neglected variations in the inertia matrix would be regarded as disturbance as well.

According to (2.21) and (2.24), the control torques are computed as;

$$\tau = J(q)^T R_c(\theta_n)[f^n \quad f^t]^T \quad (2.45)$$

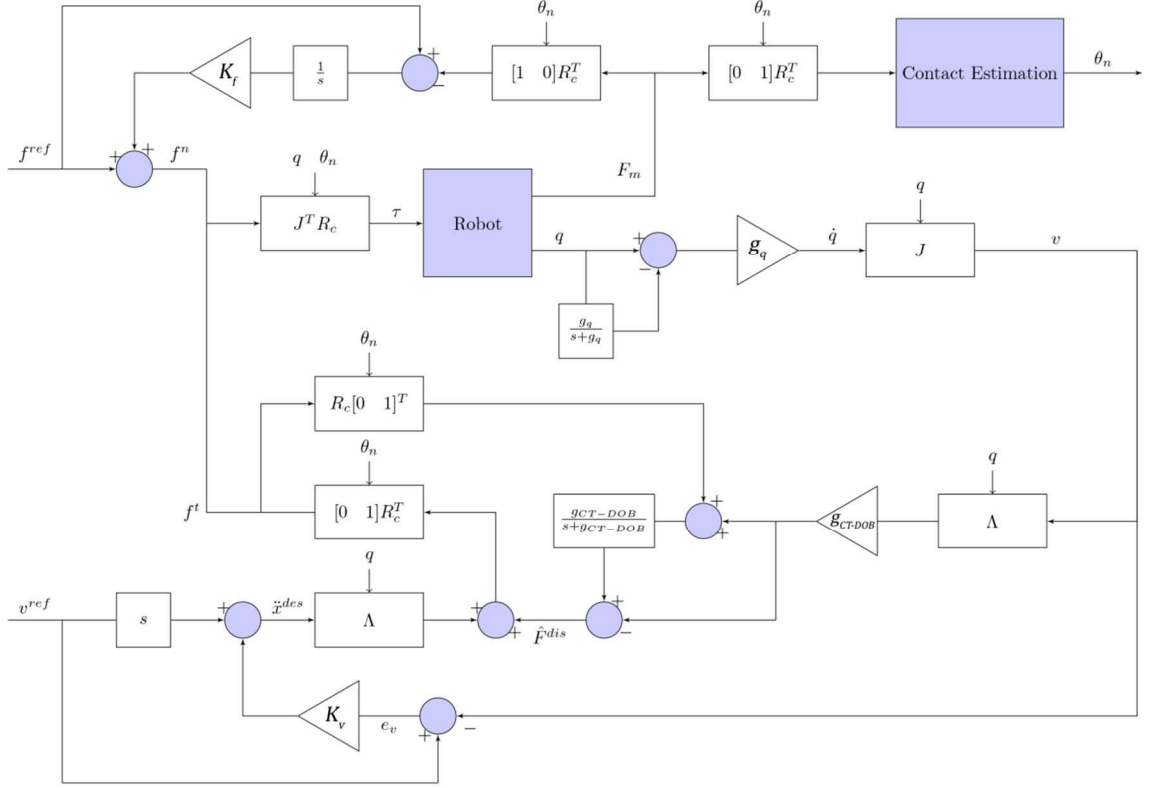


Figure 2.6: Overall block diagram of hybrid velocity/force controller

2.3.2. Determining the Contact Angle

The rotation matrix $R_c(\theta_n)$ is used extensively in the control algorithm and thus the performance of the control is highly dependent on estimation of contour normal angle θ_n . Online estimation of θ_n should be bounded to avoid drifting; and it should be continuous inside defined boundaries in order to guarantee smooth velocity reference and motion even if the tracked contour exhibits discontinuities. The following iterative method is introduced for online estimation of the contact normal angle;

$$\theta_n(k+1) = \text{sat}(\theta_n(k) + \text{sgn}(v_c)K_\theta([0 \ 1]R_c(\theta_n)^T F_m - f_{bias}^t), \pi) \quad (2.46)$$

In (2.46); $\text{sat}(u, \varphi)$ is a saturation function which keeps the input u inside the range $[-\varphi, \varphi]$, sgn refers to the signum function, v_c is the contour tracking velocity command, K_θ is the learning parameter and f_{bias}^t denotes the bias force in tangential direction. The idea is that the contact angle should be estimated and the trajectory should be generated such that the robot would be forced to move away from tangential contact since by definition of the contour coordinate frame, there should not be any

measured contact force along the tangential direction except friction; and it would be forced to keep contact because the force sensor measures the inertial forces acting on the tool as well which are in the opposite direction of tangent motion, meaning that the measured tangent force would always be negative without contact. Setting the bias force as zero is sufficient for purely contour tracking purposes where the normal force and thus the kinematic friction is low. In order to realize additional tasks during contour tracking such as grinding, deburring, or cutting, appropriate bias force should be selected considering the potential tangent forces associated with the given task.

Since this is an iterative method, an initial value is needed for θ_n . This initial value is set during the initial contact with the workpiece. If the initial contact is stable and the resulting impact forces are low, the contact angle can be accurately calculated from the force measurements $F_m = [f_x \ f_y]^T$ using the equation:

$$\theta_n = \text{atan2}(f_y, f_x) \quad (2.47)$$

The equation (2.47) is not suitable for online calculation of θ_n since it depends solely on the current force measurements, the calculation is prone to discontinuities due to possible impact forces and noise associated with force measurements. Such discontinuities would result in abrupt changes in the contour tracking trajectory. Additionally, if the workpiece edges are rough, (2.47) would not give an accurate estimation as it does not account for contact friction.

Chapter 3

3. EXPERIMENTAL SETUP, IMPLEMENTATION AND RESULTS

This chapter describes the experimental setup, presents some issues faced in the implementation and the methods used for overcoming said issues. It presents extensive results to highlight the effect of certain control parameters; experiments done with different contour tracking velocities and different normal force commands; and comparison of the used control method with dynamics based and conventional PI velocity control for the contour tracking task.

3.1. Experimental Setup

The experimental setup consists of a two degree of freedom direct drive planar manipulator controlled by a dSPACE 1102 DSP-based system. Controllers, trajectory generators, motion commands and other software routines are written in C programming language, compiled and downloaded to the DSP. The code is processed at 1 kHz frequency. Furthermore, a user interface has been created in dSPACE ControlDesk environment to interact with the robot and change certain parameters like desired velocity, desired force and controller gains in real-time. The robot is actuated by Yokogawa Dynaserv servomotors that exist at the two joints. Signals are sent from the DSP to the motor drives in order to generate required amount of torques at the joints. The sent signals are amplified at the drives by a predetermined gain and accepted as voltage commands. The maximum torque is produced with ± 8.5 V as the voltage command. The maximum torque capacity of the motor at the base is 200 Nm and that of

the motor at the elbow is 45 Nm. The gain of the motor drives was set to 10. Thus the signals to be sent to the motor drives, considering the robot is direct drive, are;

$$u_1 = 0.85 \frac{\tau_1}{200} \quad (3.1)$$

$$u_2 = 0.85 \frac{\tau_2}{45} \quad (3.2)$$

Forces at the tooltip and joint positions are measured. Joint positions are provided by the encoders of the servomotors with a resolution of 1024000 pulses/rev at the base and 655360 pulses/rev at the elbow. External force measurements are obtained by an ATI Gamma six-axis force/torque transducer attached on the second link of the robot, at the “wrist”. Hence any force exerted on a point above the wrist can be sensed by the transducer.

The robot dynamics parameters referred in equations (2.3) and (2.4) are computed from the CAD model of the robot. Rotor inertias and motor weights are obtained from the manufacturer’s documentation.

Table 3.1: Dynamics Parameters

m_1	18.94 kg	m_2	3.51 kg
l_1	0.4 m	l_2	0.37 m
l_{c1}	0.2737 m	l_{c2}	0.1691 m
I_1	0.67 kgm ²	I_2	0.07 kgm ²
J_1	0.167 kgm ²	J_2	0.019 kgm ²

The contour of the workpiece used for the experiments (Fig 3.1) starts with a 5 cm line with 60° contact normal angle, ends with a 5 cm line with 120° contact normal angle and the 25 cm long arc in between covers a contact normal angle range of [45°,135°]. It is created by laser cutting a 400mm x 300mm x 10 mm DuroFoam sheet. It has high stiffness such that it does not deform or bend during pressing with forces up to 50 N. The edges describing the contour, however, is quite rough due to the used material not being appropriate and thin enough for the cutting machine used to shape its contour.



Figure 3.1: Image of the workpiece showing entirety of its contour

3.2. Implementation Issues

Both force sensor and motor encoders exhibit significant noise. Force sensor also has substantial bias. This bias is removed simply by assuming the initial readings of each axis of the sensor as offset while the robot is away from contact and stationary, then subtracting them from the force sensor readings for the rest of the run of the code. The measured forces are also low-pass filtered. The noise of the motor encoders itself does not pose significant problem but it affects the disturbance observers as touched upon in section 1.4. Also, joint velocities, which are not directly available as measurement, are needed for the realization of proposed control. Direct discrete differentiation of motor encoders readings would amplify the associated noise and cause oscillations and instability if high derivative gains in feedback control or high disturbance observer gains are used. In order to remedy that, the following method has been used to estimate the joint velocity vector \dot{q} ;

$$q_{filt} = q \frac{g_q}{s + g_q} \quad (3.3)$$

$$\hat{q} = g_q(q - q_{filt}) \quad (3.4)$$

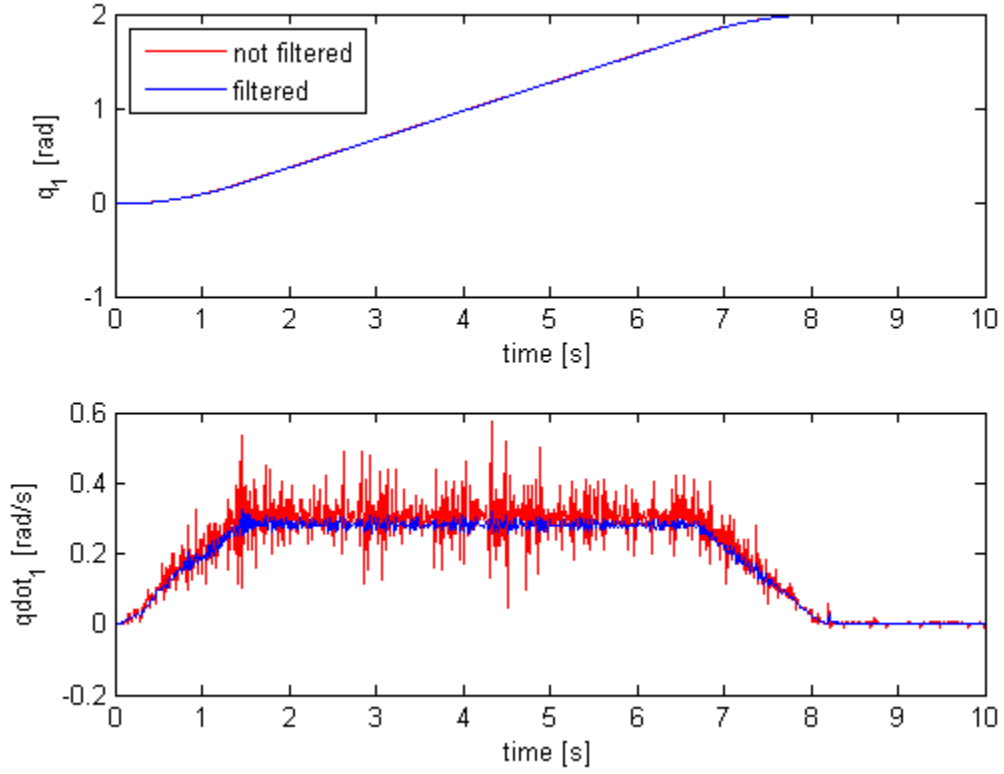


Figure 3.2: Comparison of the filtered and raw joint angle measurements

The effect of this procedure is demonstrated on Fig. 3.2 where the cut-off frequency was set to 10 Hz. For the experiments, 3 Hz and 6 Hz cut-off frequency has been used. This joint velocity estimation and disturbance observer, as well as the filtering of the force measurements require implementation of the low-pass filter. Discretization of the low-pass filter is performed by forward Euler approximation: $s \leftarrow \frac{1}{T}(z - 1)$ where T is the cycle time. The discrete equivalent (3.5) is obtained and used in the implementation. In (3.5), g is the low-pass filter cut-off frequency in rad/s.

$$x_{fit}[k + 1] = (1 - gT)x_{fit}[k] + gTx[k] \quad (3.5)$$

If the tooltip gets jammed during contour tracking for some reason like contact normal angle not being calculated properly or the required motion being out of the reach of the robot, the disturbance observer would regard the lack of desired motion to be caused by disturbance and the estimated disturbance term \hat{F}^{dis} would increase rapidly due to windup, which may cause instability or exertion of too much force on the workpiece. Therefore, the computed tangent force control term f^t is saturated with the limit of 50 N.

During switching of the control at contact, the tooltip slightly slides on the contour in the opposite direction of the desired contour tracking velocity and the measured tangent force becomes negative due to tooltip moving opposite of the tangent direction shown on Fig 2.5. This results in incorrect estimation of the contact normal angle. Measures have been taken to make the contact estimation blind to mentioned sliding motion by deactivating it until a certain velocity is reached in the correct direction. Since the initial value of the contact normal angle is set by the equation (2.47) before the switching of control, the controller receives correct velocity references that generate motion along the contour.

3.3. Experimentation and Results

The force feedback gain K_f and the velocity feedback gain K_v have been set to 0.9 and 10 respectively, and kept constant for the majority of experiments. The effects of joint angle measurement low-pass filter cut-off frequency g_q , disturbance observer gain g_{CT-DOB} and the learning parameter K_θ for contact estimation have been investigated. Moreover, experiments have been carried out for different values of normal force and contour tracking velocity commands.

3.3.1. The Effect of Cut-Off Frequency

The cut-off frequency of the low-pass filter used to filter the encoder readings, which are used in the estimation of joint velocities, is highly effective in the performance, robustness and stability of the disturbance observer [2]. A stricter low-pass filter with lower cut-off frequency would remove noise in a larger frequency range. However, as the cut-off frequency decreases, the time delay associated with the low-pass filter increases. Too much delay may cause inaccurate motion and instability. The noise that cannot be removed by filtering is picked up by the disturbance observer, regarded as disturbance and amplified by the disturbance observer gain. Hence, having lower cut-off frequency enables usage of higher disturbance observer gain.

Although 6 Hz cut-off frequency was being used for general motion, it has been lowered to 3 Hz during contour tracking for the majority of experiment to make the usage of higher disturbance observer gains possible. Resulting increase in time delay does not pose a problem since the velocities are low during contour tracking. Several experiments have been done with 6 Hz cut-off frequency and it was experimentally seen that g_{CT-DOB} could not be safely increased further than 150 due to oscillations in motion.

Experimental results (Fig 3.3 and 3.4) are obtained by setting g_{CT-DOB} to 150 and with 5 mm/s contour tracking velocity command¹. Fig 3.3 shows the increased chattering of the control torques when the cut-off frequency is increased to 6 Hz from 3 Hz. This results in higher frequency oscillations of the tooltip velocity and increase in the amplitude of instantaneous velocity measurements (Fig 3.4).

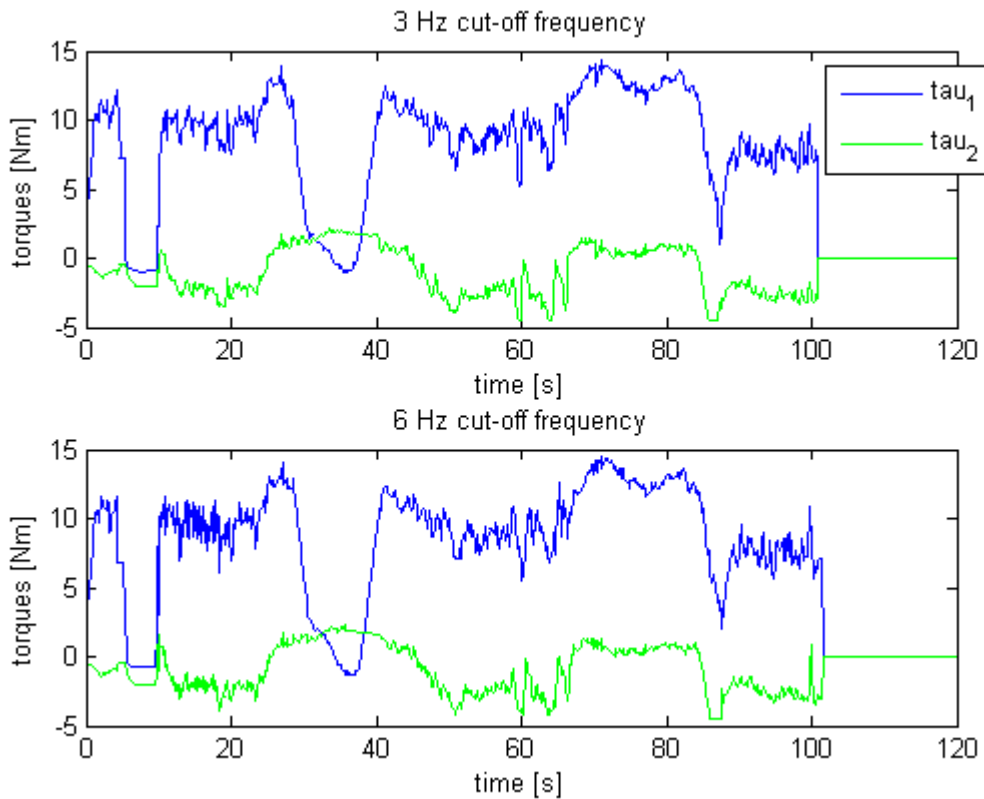


Figure 3.3: Cut-off frequency comparison - control torques

¹ The velocity references in the experiments are created with 1 mm/s² acceleration up to the velocity command instead of a step, in order to ensure differentiable v^{ref} due to the \dot{v}^{ref} term seen in equation (2.40).

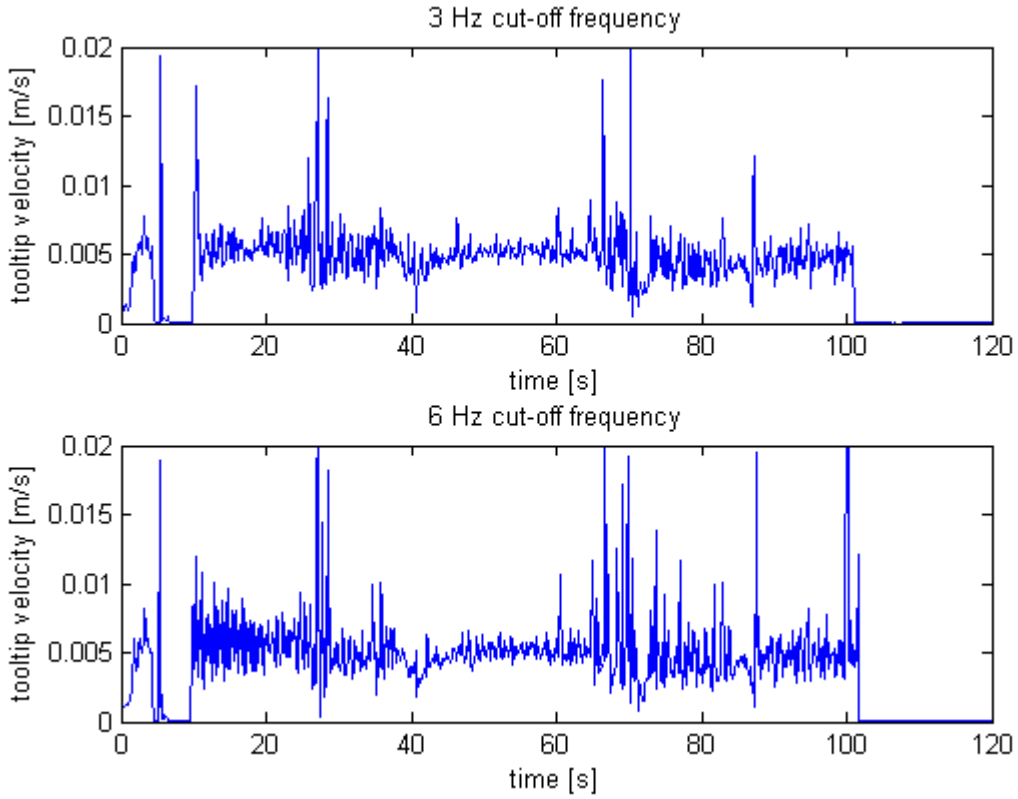


Figure 3.4: Cut-off frequency comparison - tooltip velocity

3.3.2. The Effect of Disturbance Observer Gain/Bandwidth

The set of experiments presented in this section is performed with 10 N normal force command, 3 mm/s contour tracking velocity command, $K_{\theta}=0.005$ and disturbance observer gains [150, 200, 225].

The force tracking performance is shown on Fig. 3.5. The variation of disturbance observer gain is not particularly effective on the applied normal force since control in the normal direction is governed by integral force feedback control. However, as motion response to disturbances becomes more robust due to higher disturbance observer gains, integral control seems inadequate to respond fast enough; hence the drop of applied normal force at instantaneous velocity peaks.

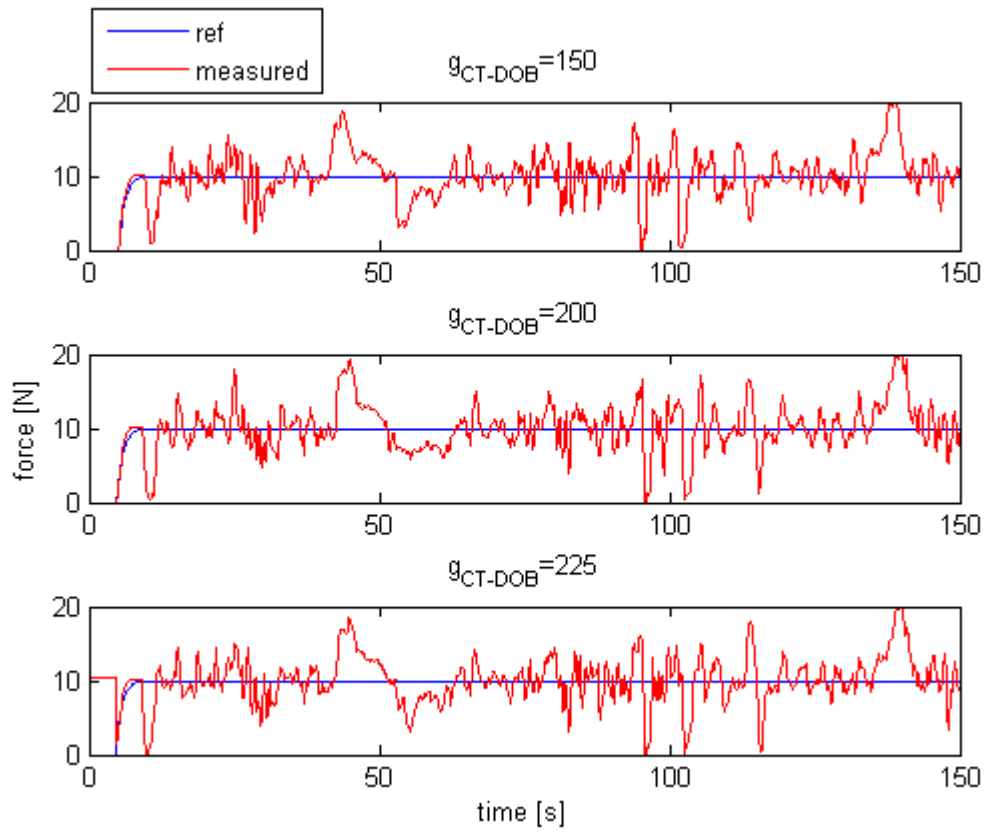


Figure 3.5: Disturbance observer gain comparison- normal force tracking

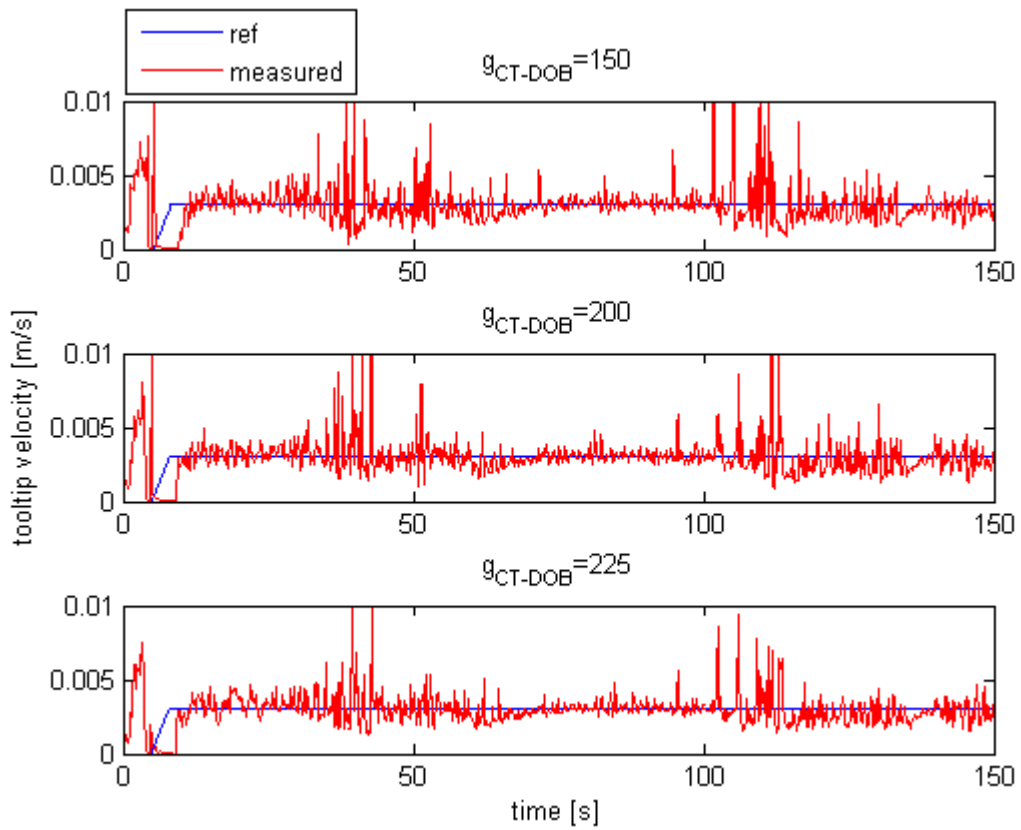


Figure 3.6: Disturbance observer gain comparison - velocity tracking

Increase in disturbance observer gain improves the velocity tracking performance (Fig. 3.6) of the hybrid velocity/force control. The motion response of the robot is especially improved when the tracked contour direction changes. For instance, between 50-55 second marks, the tooltip reaches the tip of the arc of the tracked contour. It is seen that the overshoot of the tooltip velocity is lessened with the increase of disturbance observer gain. Using low disturbance observer gains result in loss of contact at the mentioned point of the contour, particularly with higher tracking speeds. It is desirable to set the disturbance observer gain as high as possible for compensation of disturbances in wider frequency range. However, the disturbance observer gain/bandwidth is limited in the experiments mostly due to the noise associated with the estimated tooltip velocity. The gains used for the presented results were experimentally selected to ensure robust control with minimal oscillations in motion.

The estimated contact normal angle plot during these experiments is also given (Fig 3.7) for the purpose of showing the contour direction at different times.

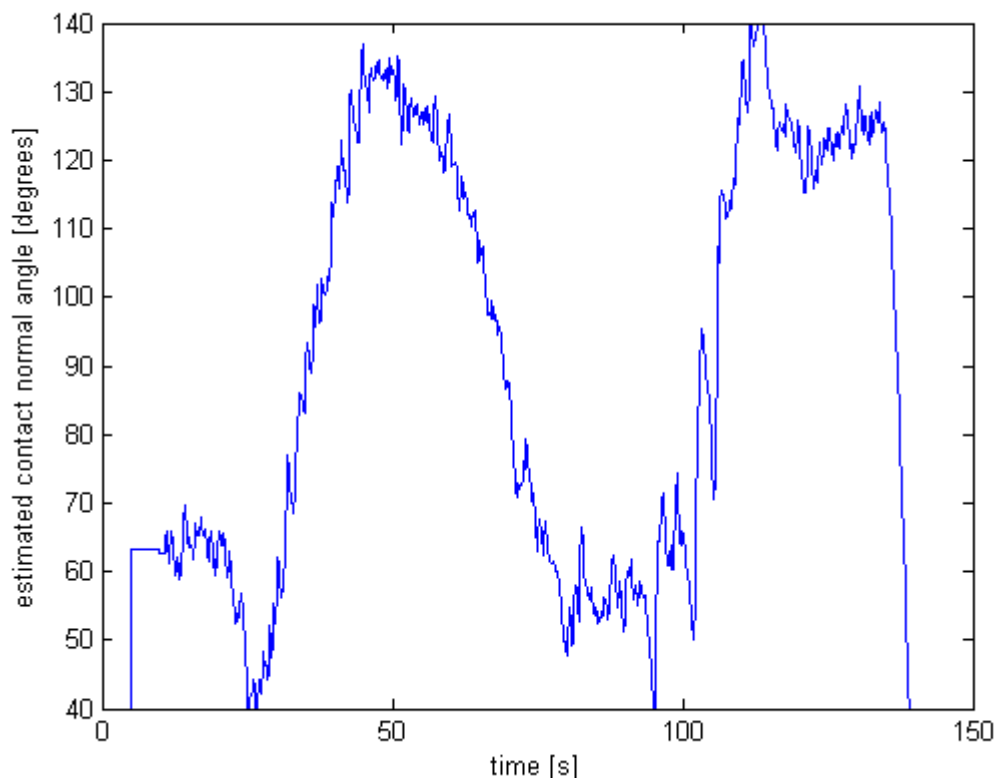


Figure 3.7: Disturbance observer gain comparison - estimated contact normal angle

3.3.3. The Effect of Contact Estimation Learning Parameter

The set of experiments presented in this section is performed with 10 N normal force command, 5 mm/s contour tracking velocity command, $g_{CT-DOB}=150$; and with K_θ values 0.005 and 0.01.

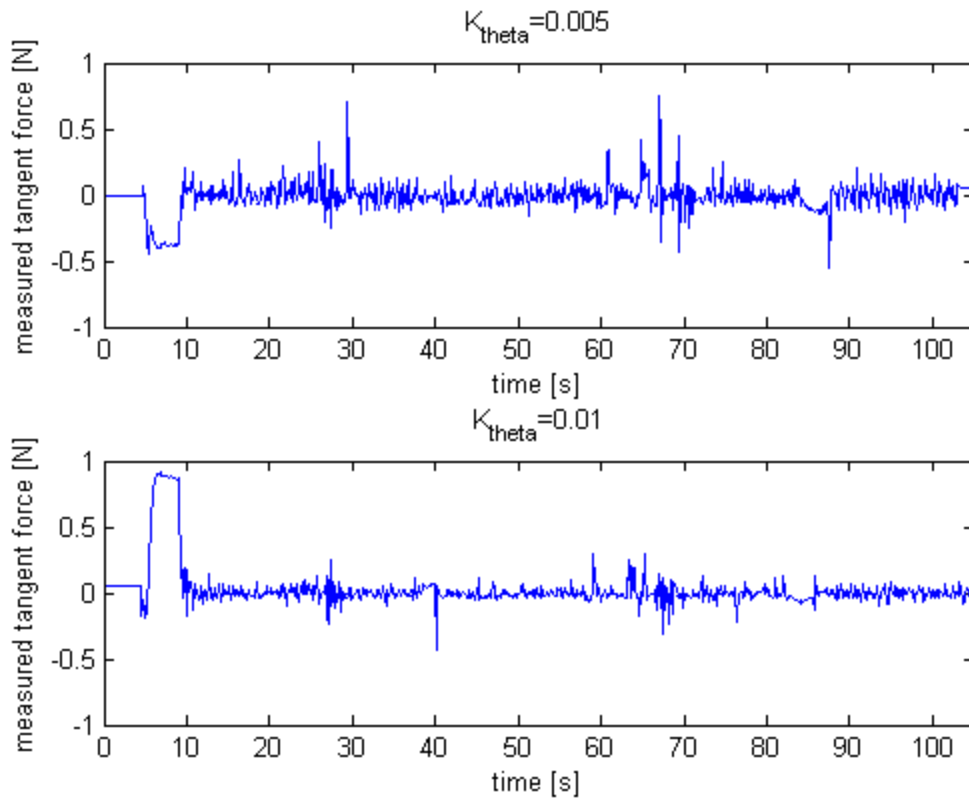


Figure 3.8: Learning parameter comparison - measured tangent force

Recall that the contact estimation procedure is blind to the measured tangent forces until motion starts which happens right before the 10 second mark during these experiments. The measurements before that moment does not affect the estimated contact normal angle. The measured tangent forces (Fig. 3.8) decrease and get closer to zero as the K_θ value is increased to 0.01 from 0.005 due to faster estimation of the contact angle normal. This means that the velocity references coming from the estimated contact angle are better at pushing the tooltip away from the detected tangent forces which is desirable. However, having high K_θ may also result in estimating the contact normal angle significantly larger or smaller than it really is; which is demonstrated on Fig 3.9

where directions of the velocity references are shown during contour tracking at the middle part of the workpiece. The tooltip is moved away from the contour due to contact normal angle being estimated larger than its real value. Notice that, at that moment, θ_n stops being updated due to loss of contact for a small period of time (Fig. 3.10). This problem may be avoided by having an appropriate positive f_{bias}^t value. In that case, the velocity reference would be generated such that the measured tangent force would be around the set bias. Then the motion would be less prone to loss of contact.

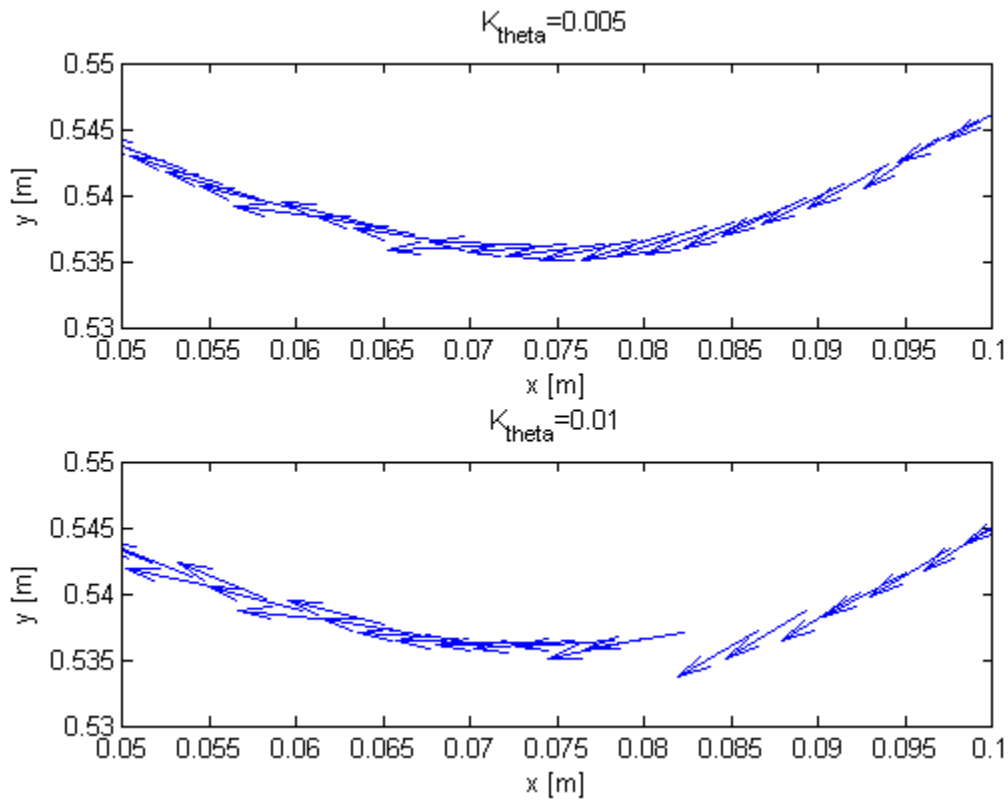


Figure 3.9: Learning parameter comparison - velocity reference directions at the tip of the contour

The negative spike in the measured tangent force, seen on Fig. 3.8, when K_θ is set to zero, corresponds to the moment the tooltip reaches the corner of the workpiece towards the end of the contour (right corner on Fig 3.1). The sudden change in the direction of the contour at the corner results in an instantaneous negative tangent force. When K_θ is set to 0.01, such a spike does not occur due to faster estimation of the contact normal angle. The generated velocity reference directions around the mentioned corner can be seen on Fig. 3.11.

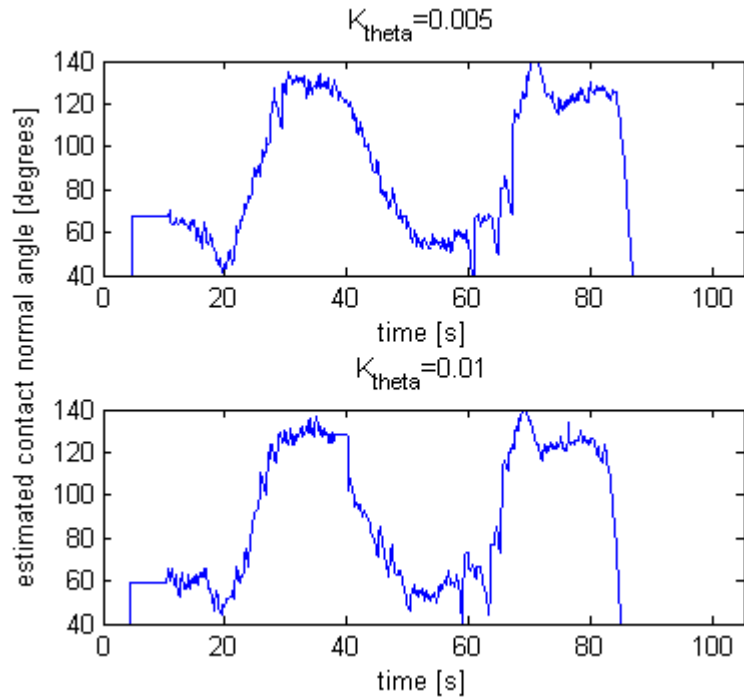


Figure 3.10: Learning parameter comparison - estimated contact normal angles

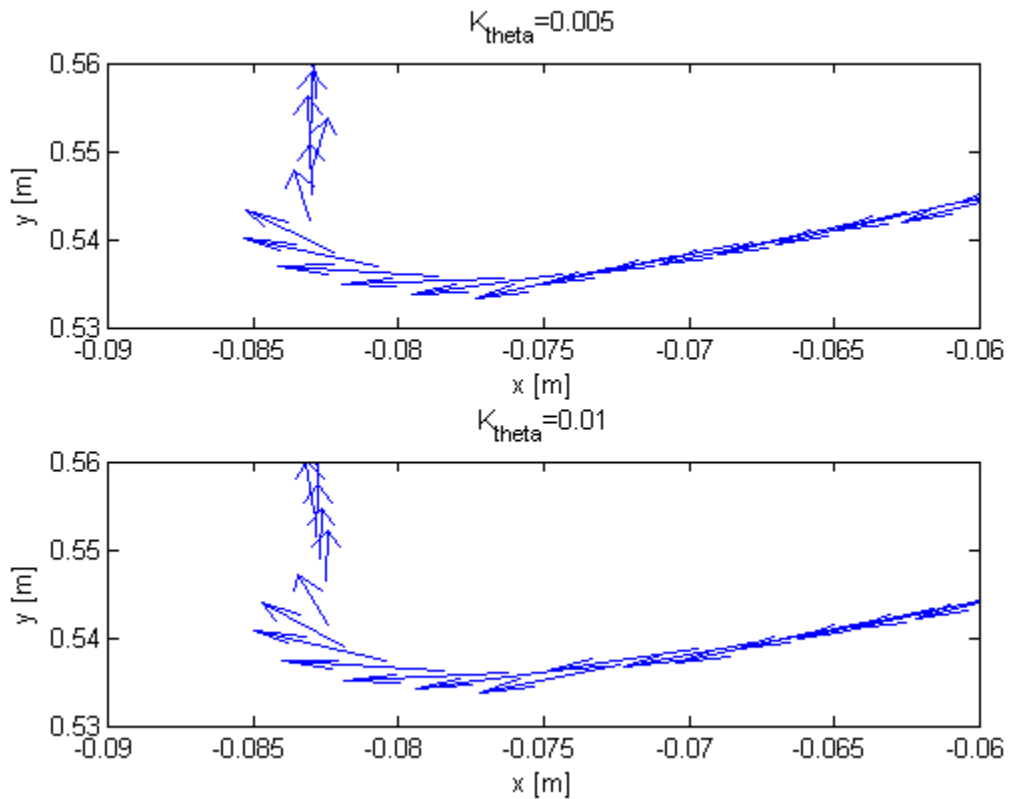


Figure 3.11: Learning parameter comparison - velocity reference directions at the corner of the contour

3.3.4. Demonstration of the Contribution of Disturbance Observer

In this section; the hybrid velocity/force control with disturbance observer as presented will be compared with hybrid velocity/force control where the disturbance observer is substituted with dynamics based or conventional integral feedback control. Addition of dynamics based integral control means simply adding the integral velocity feedback term to \ddot{x}^{des} . Then the equation (2.41) becomes;

$$\ddot{x}^{des} = \dot{v}^{ref} + K_v e_v + K_I \int e_v dt \quad (3.6)$$

The multiplication of \ddot{x}^{des} with the operational space inertia matrix $\Lambda(q)$ in computing the tangent control force remains and thus the robot dynamics is considered. Conventional integral feedback control refers to applying PI control to velocity feedback coming from both dimensions of the operational space;

$$u_{PI} = K_v e_v + K_I \int e_v dt \quad (3.7)$$

Then, using the computed outputs of the PI scheme to compute the tangent control force as follows;

$$f^t = [0 \quad 1] R_c(\theta_n)^T u_{PI} \quad (3.8)$$

In this approach robot dynamics or the configuration of the robot is not considered. Conventional PI proved to be quite ineffective in enforcing contour tracking during experiments. Extensive tuning of the controller gains for both x and y dimensions may yield better results. However, PI tuned for the contour tracking task at some area of the workspace would not work as well at some other part of the workspace since the robot configuration information is not used. Control effort needed to minimize error in x and y dimensions vary with respect to the change of robot configuration. The required information for scaling the control is carried by the Jacobian $J(q)$ which is embedded in the operational space inertia matrix.

The control parameters (where applicable) used for the experiments of this section are given in Table 3.2. The designed disturbance observer based velocity control will be

referred as “P+DOB” for simplicity, as it is essentially proportional velocity feedback control with disturbance observer.

Table 3.2: Control Parameters

	f_c	v_c	K_f	K_v	K_I	\mathcal{G}_{CT-DOB}	K_θ
P+DOB	10 N	3 mm/s	0.9	10	-	200	0.005
Dynamics based PI	10 N	3 mm/s	0.9	100	200	-	0.005
Conventional PI	10 N	3 mm/s	0.9	100	200	-	0.005

Detailed comparison of the PI control described in (3.7) and (3.8) is not necessary since it fails to enforce contour tracking with the used gains. The force (Fig. 3.12) and velocity (Fig. 3.13) plots are presented for the sake of completeness. Significant time passes until enough control effort is accumulated by the integral term to overcome static friction and start motion, then the velocity overshoots substantially resulting in clumsy motion. The second velocity peak seen on Fig 3.13 exceeds the set maximum velocity limit and the robot stops itself for security.

Figures 3.14-17 compares the P+DOB and dynamics based PI. The main contribution of the disturbance observer is seen in the velocity tracking performance (Fig. 3.15). It can be seen that the average amplitude of oscillations is significantly lower with the P+DOB, the tooltip tracks the commanded contour tracking velocity more precisely. Especially between 40-75 second marks where the tooltip is “climbing out” of the first concavity of the contour, it can be seen that dynamics based PI struggles to maintain continuous velocity as the tooltip stalls for brief moments (just before and after the 50 second mark); whereas the tooltip never stalls during contour tracking with P+DOB. The average velocity achieved with P+DOB is 2.966 mm/s while it is 2.684 mm/s with dynamics based PI. The RMS of velocity error with dynamics based PI is 2.081 mm/s while it is 1.211 mm/s with P+DOB; it is reduced by %42.

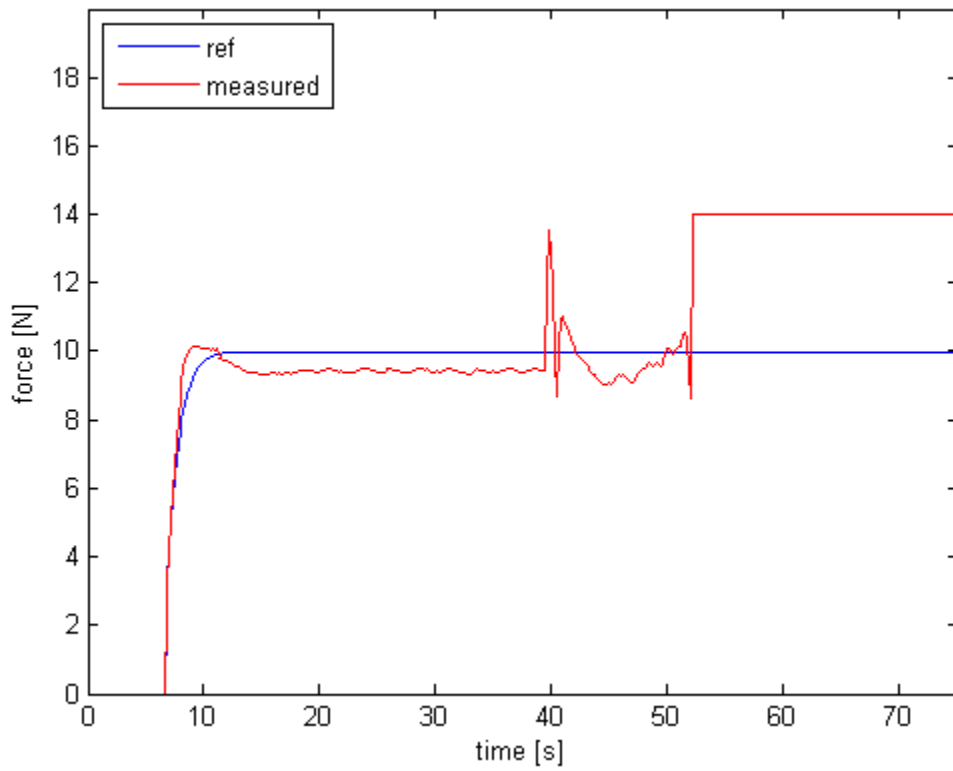


Figure 3.12: Normal force response for conventional PI

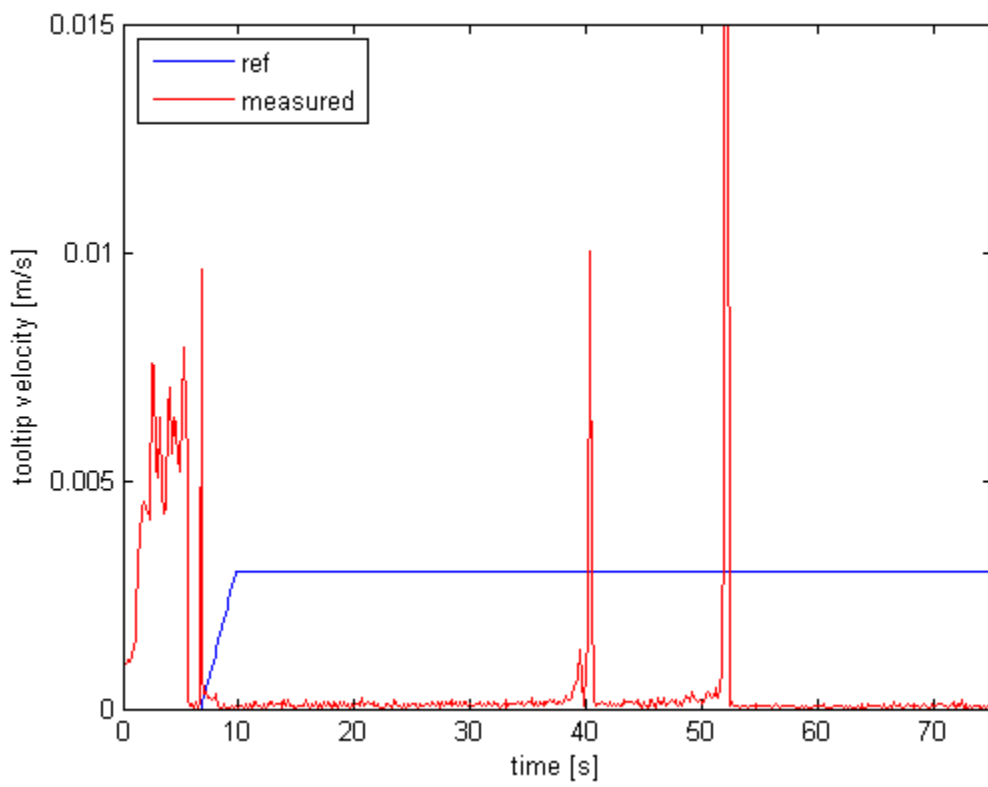


Figure 3.13: Velocity response of conventional PI

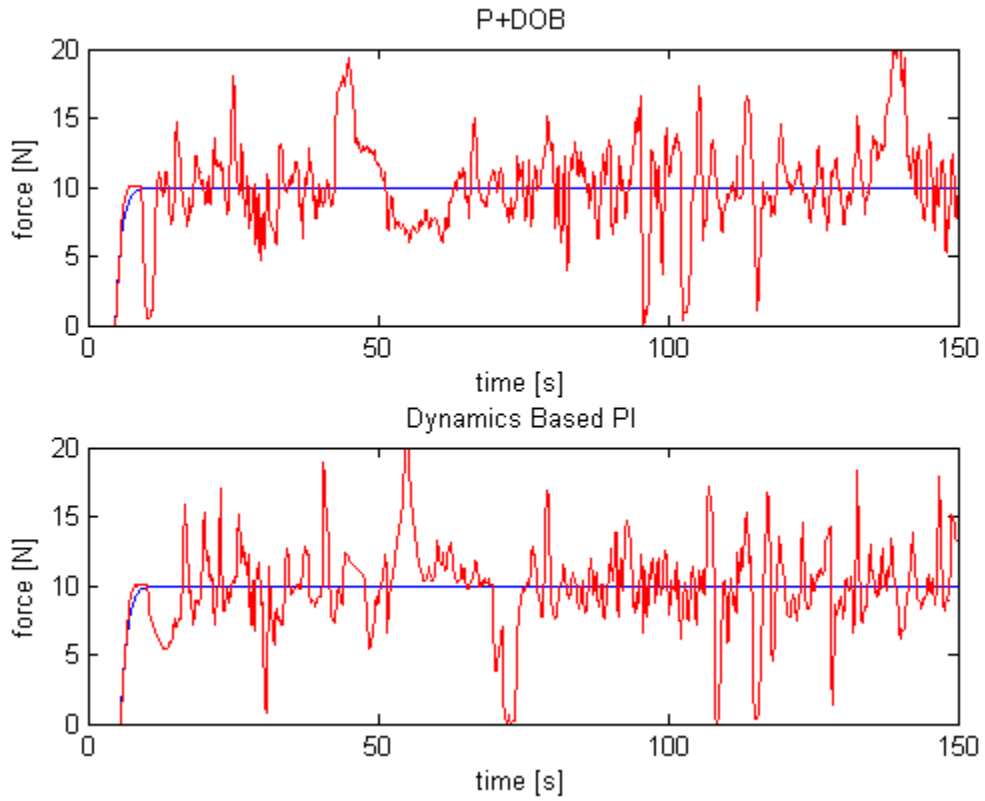


Figure 3.14: P+DOB vs. dynamics based PI – force tracking

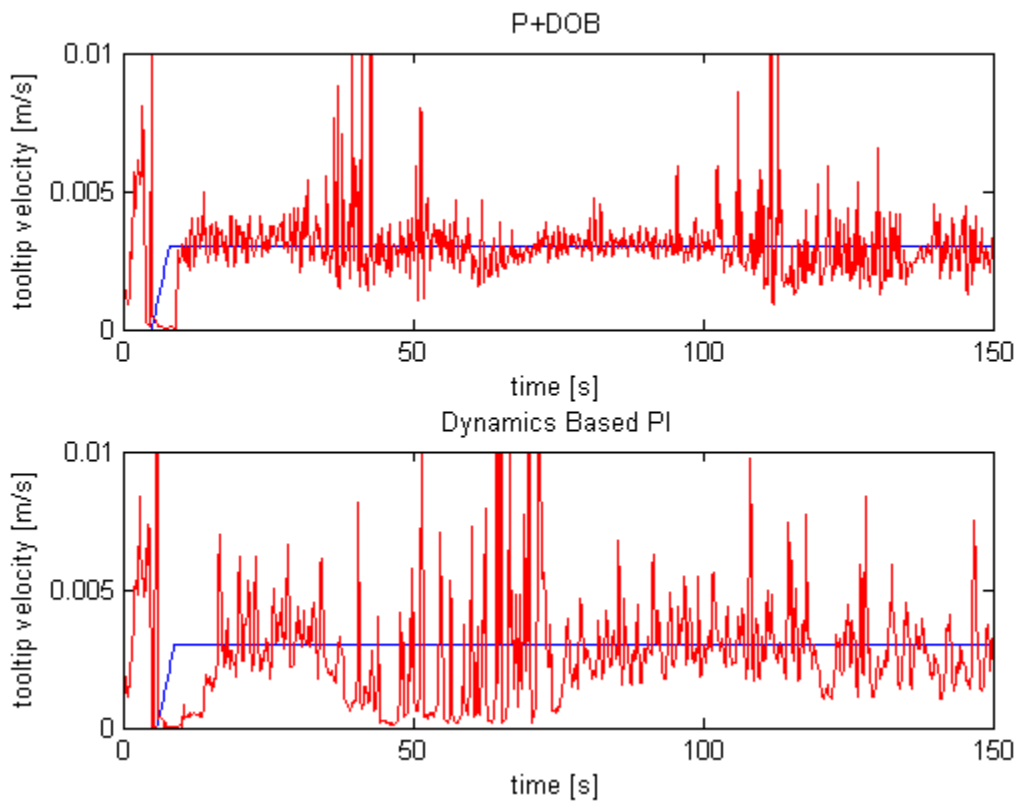


Figure 3.15: P+DOB vs. dynamics based PI - velocity tracking

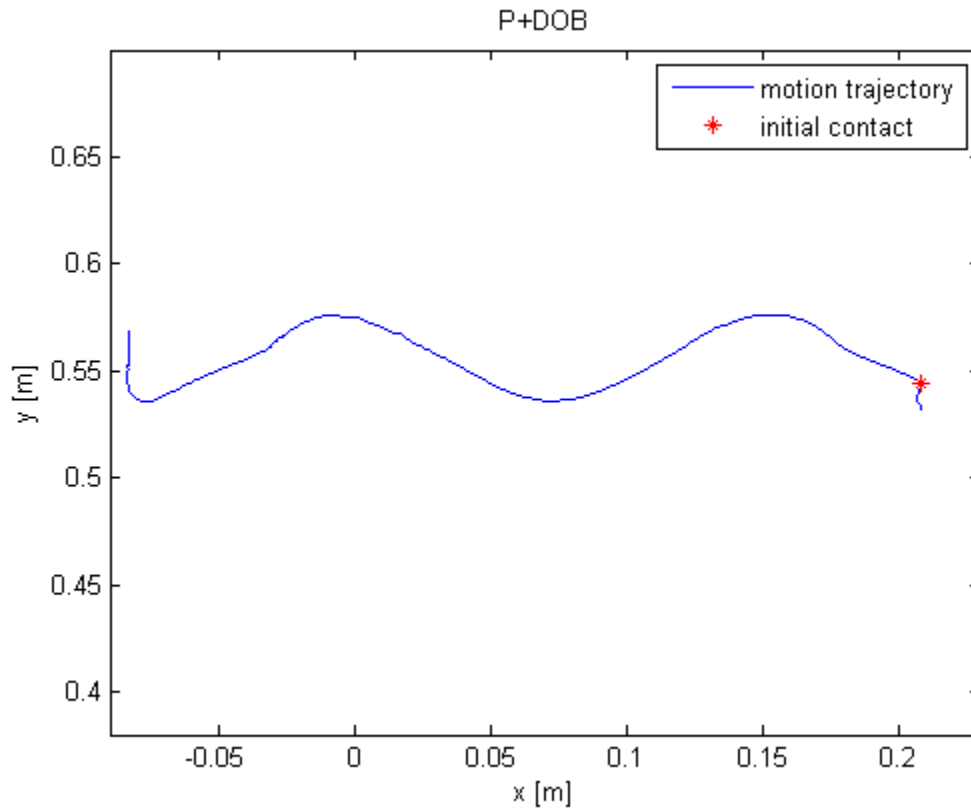


Figure 3.16: Traversed path with P+DOB

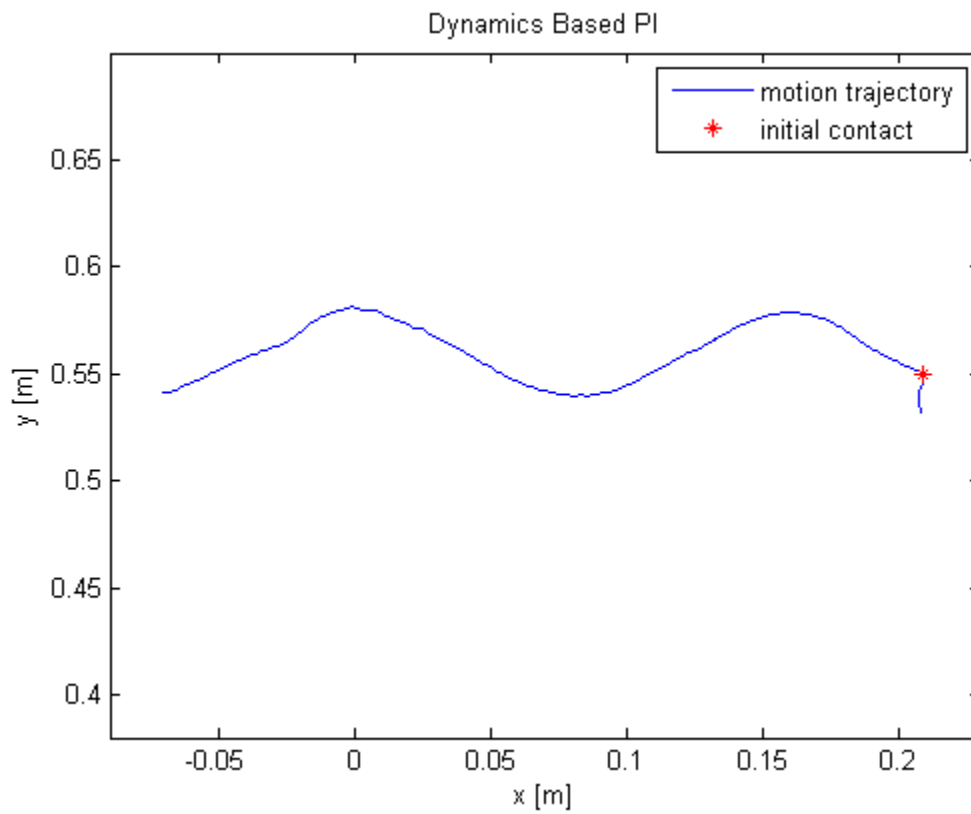


Figure 3.17: Traversed path with dynamics based PI

The force tracking performance is not significantly different since the compared methods differ in the generation of tangent control force only. However, due to reasons explained in section 3.3.2, there are slight differences in force tracking as well. The mean value of the applied normal force with P+DOB is 9.788 N while it is 9.486 with dynamics based PI. However, the RMS of force error is slightly higher with P+DOB. It is 3.336 N while with dynamics based PI, it is 3.028 N.

The traversed paths in operational space are shown on Fig. 3.16 and 3.17. They correspond to a smoothed version of the workpiece contour (Fig 3.1), since the used tooltip is circular. The data were acquired during a fixed period of experiment time of 150 seconds. Since the average velocity with P+DOB was higher, the tracked contour is longer.

3.3.5. Increasing the Normal Force and Contour Tracking Velocity Commands

The first experiment results that are presented in this section (Fig 3.18-21) are obtained when the normal force command f_c is set to 20 N while the other parameters are kept at the same values as seen on Table 3.2, P+DOB row.

It should be noted that the tooltip gets jammed at the corner of the workpiece as can be easily seen on Fig. 3.19 by the sudden drop in tooltip velocity and since the discontinuous part cannot be passed, the contact angle cannot be correctly estimated considering the contact normal exactly at the corner is undefined. The estimated contact normal angle drops to around 30 degrees which leads to both the generated normal and tangent force directions being towards the workpiece. However, the corner is passed given enough time. This is an example of the stability problem described in section 3.2. The estimated tangent disturbance (Fig. 20) rapidly increases while the tooltip is jammed which in turn results in a very high velocity spike at the moment the tooltip gets unjammed. This may result in instability if the tangent control force is not saturated. The effect of the used saturation is also seen on Fig. 3.20 as the estimated tangent disturbance cannot exceed 50 N which was the saturation limit.

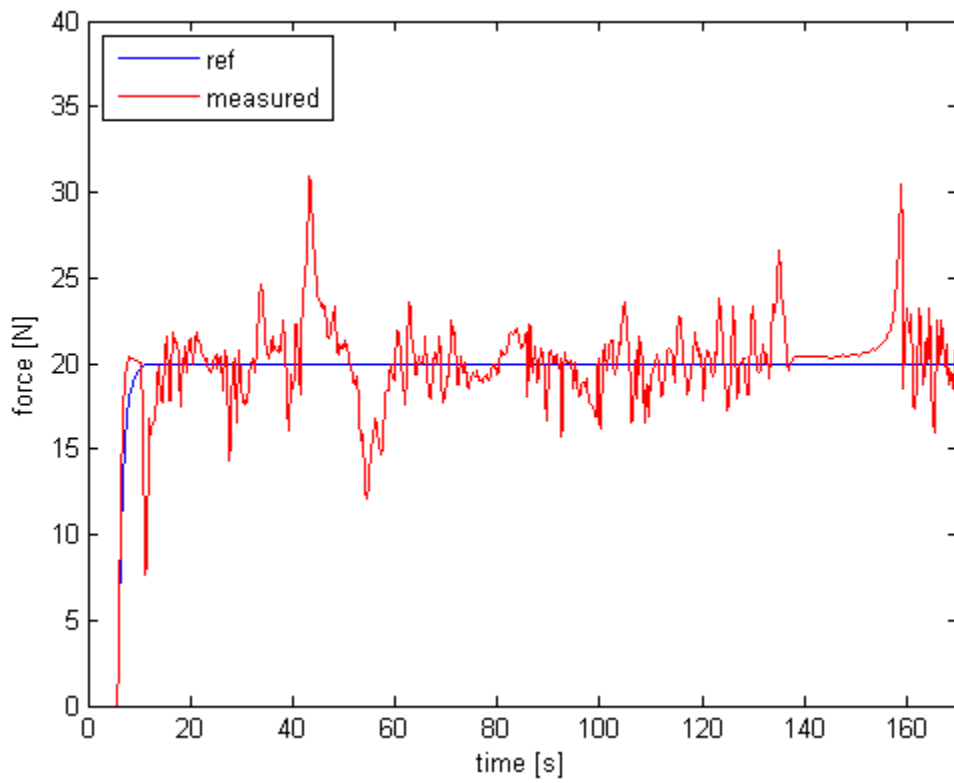


Figure 3.18: 20 N normal force command - force tracking

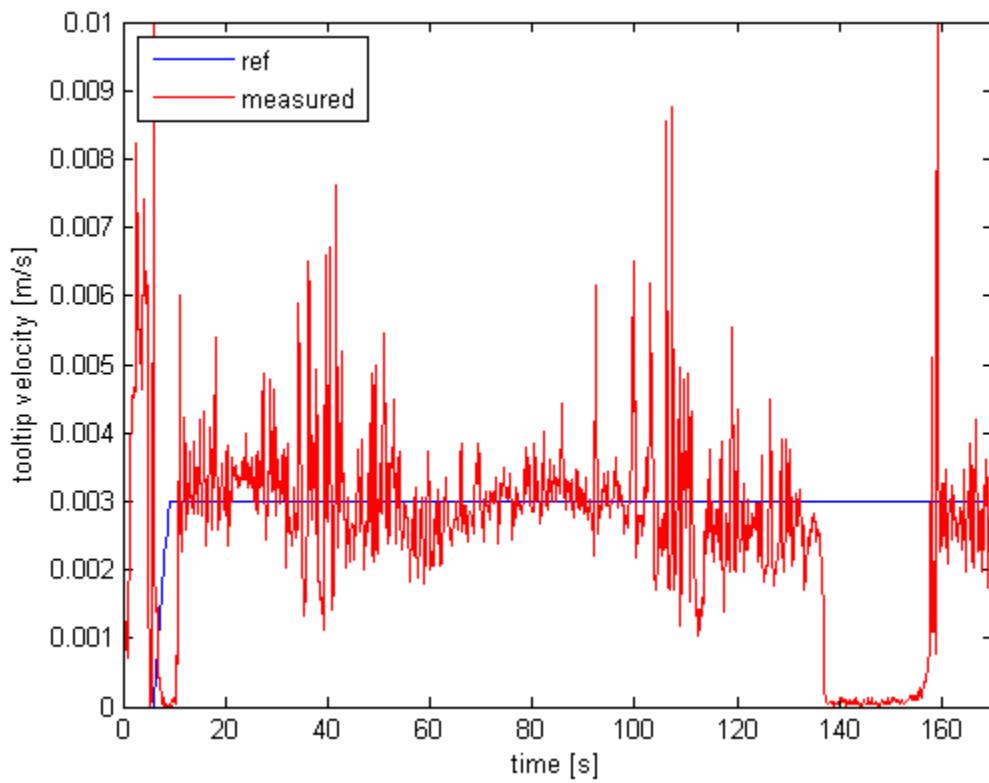


Figure 3.19: 20 N normal force command - velocity tracking

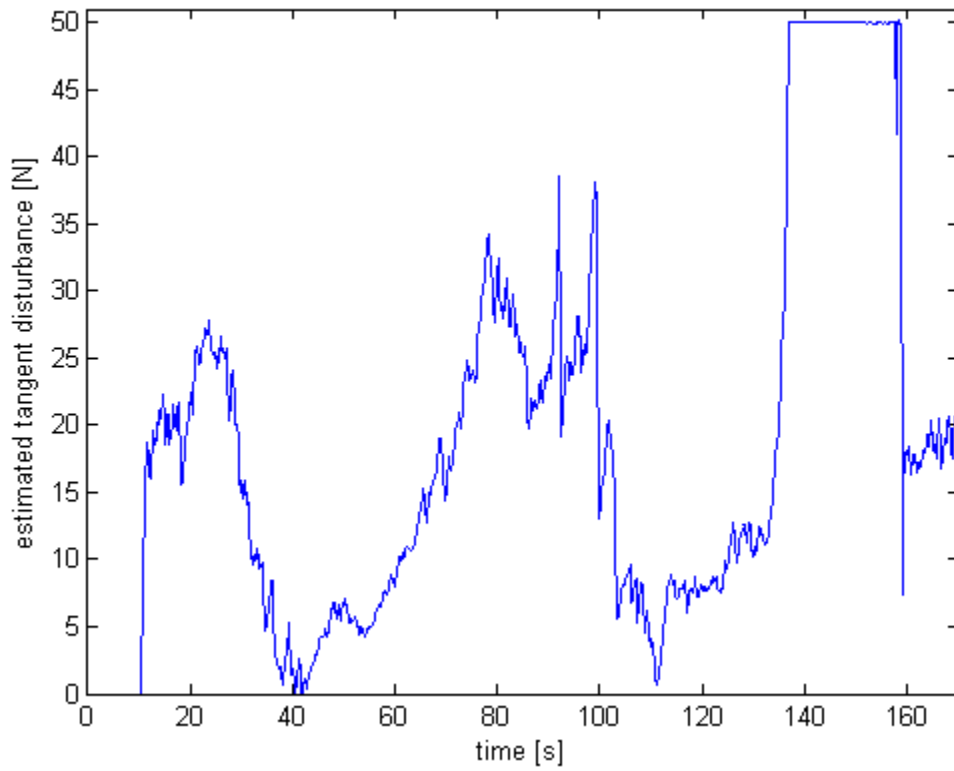


Figure 3.20: 20 N normal force command - estimated tangent disturbance

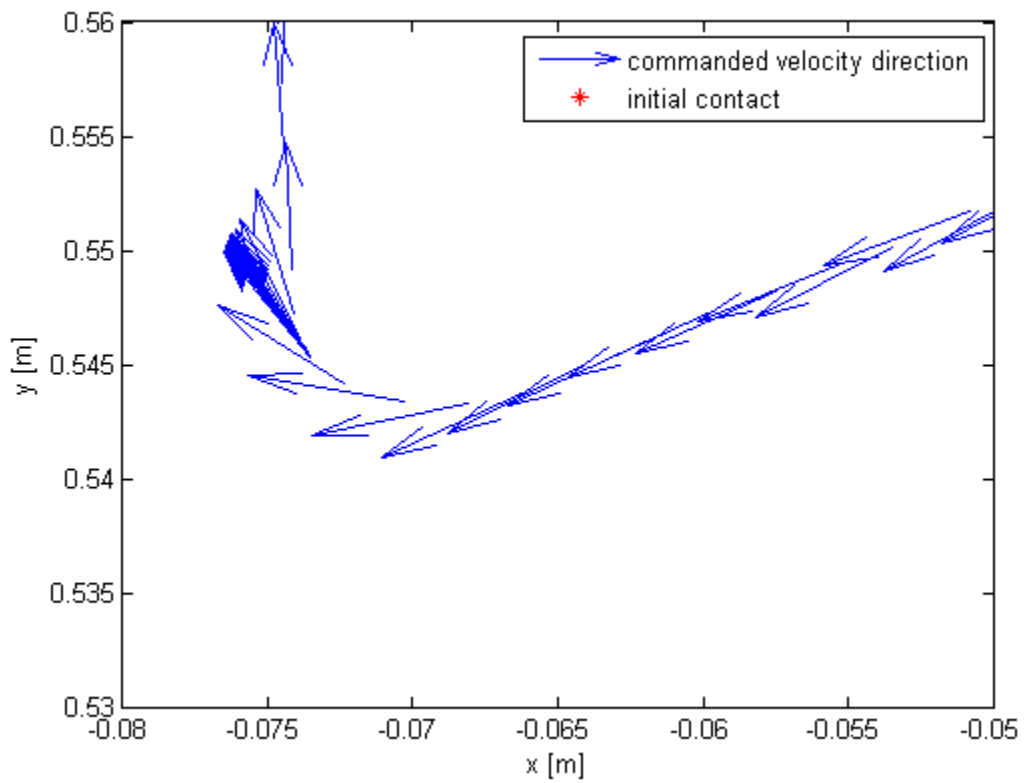


Figure 3.21: 20 N normal force command - velocity vector directions at the corner

The computed velocity references while the tooltip is jammed can be seen on Fig 3.21. Notice that while the velocity references are actually directed away from the corner, the tooltip cannot move because it has been stuck right before it passed the corner. Meaning, the velocity references actually commanding the tooltip inside the workpiece.

The next experiment results (Fig 3.22-24) are obtained when the normal force command f_c is set to 20 N, the contour tracking velocity command v_c is set to 20 mm/s, the disturbance observer gain set to 100 while the other parameters are kept at the same values as seen on Table 3.2, P+DOB row.

Substantial error in normal force is recorded, as can be seen on Fig. 3.22, due to integral force control not being fast enough to handle normal force errors at such high velocity motion. Although the measured velocity oscillation amplitudes increase, the contour is tracked without loss of contact and around the reference velocity for the most part. Tooltip jamming problem persist due to commanded normal force being 20 N. However, the contour is successfully tracked until the corner as can be seen on Fig. 3.24.

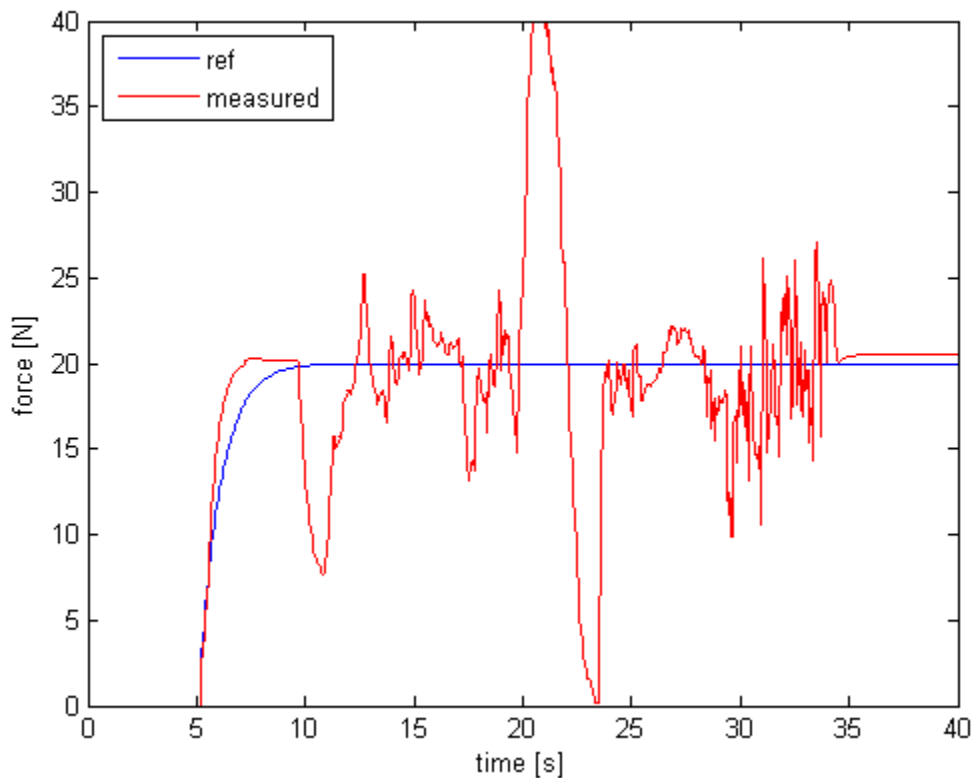


Figure 3.22: 20 mm/s contour tracking velocity command - force tracking

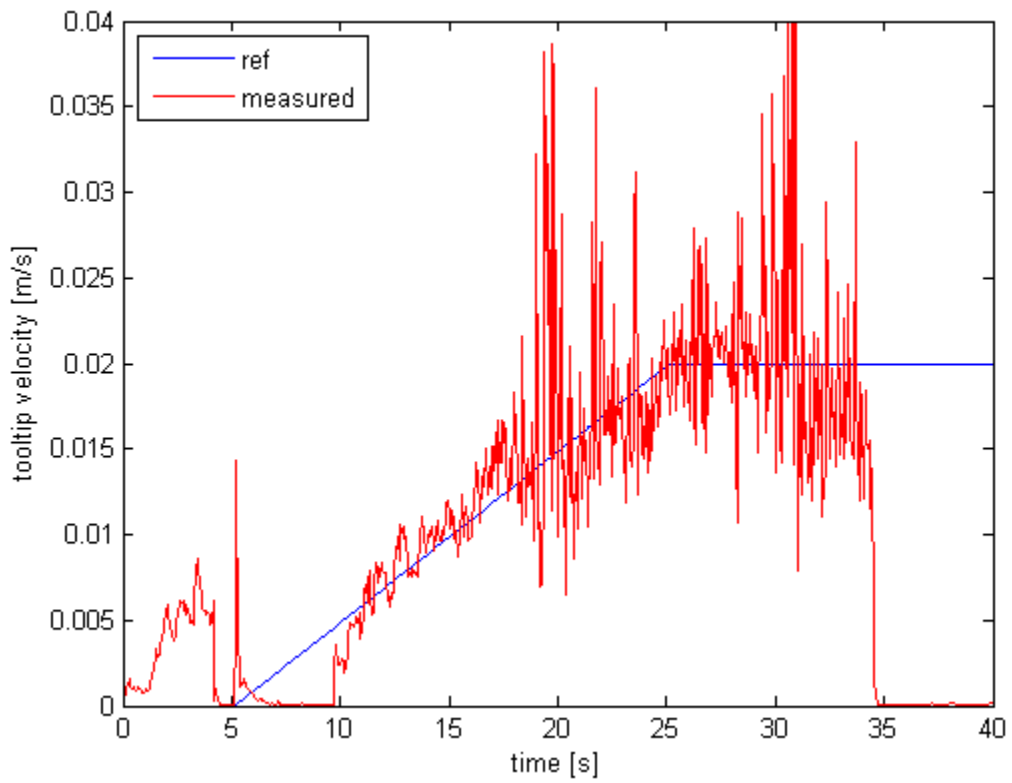


Figure 3.23: 20 mm/s contour tracking velocity command - velocity tracking

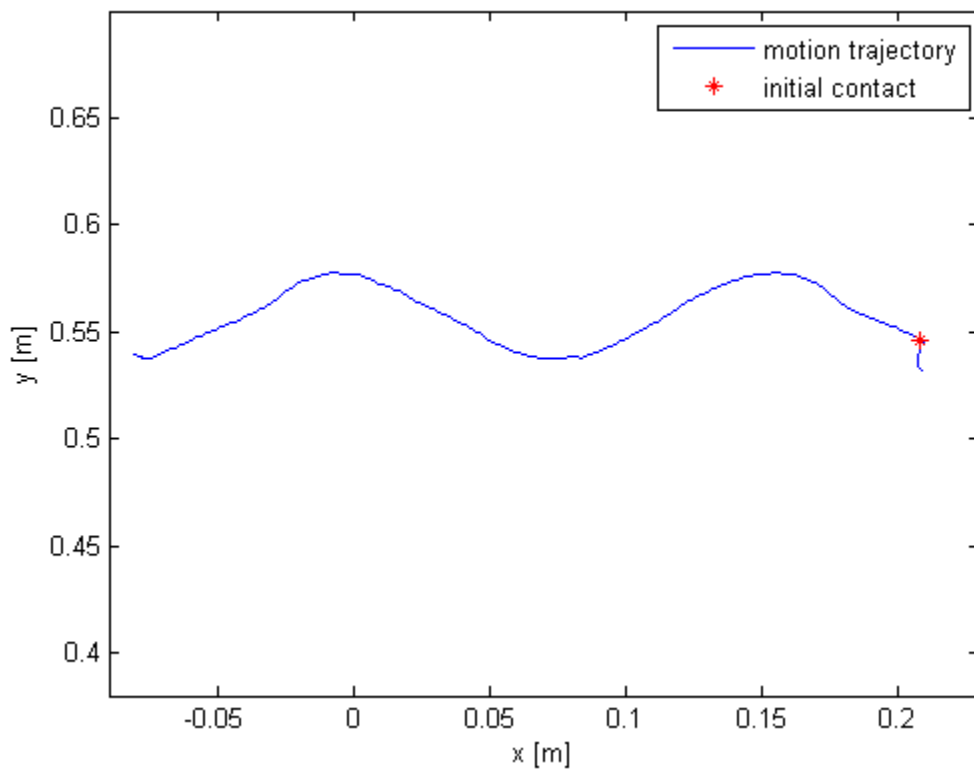


Figure 3.24: 20 mm/s contour tracking velocity command - traversed path

Chapter 4

4. DISCUSSION AND CONCLUSION

Design and implementation of a hybrid velocity/force control for the contour tracking task, employing an operational space disturbance observer constrained on the tangent direction of the contour, has been presented in this thesis along with a simple and flexible iterative method for estimating the contact normal angle. Effectiveness of the proposed methods have been validated experimentally.

The advantages of the proposed control include: no dependence on the feedback gains for disturbance compensation, hence less need for extensive tuning, complete compensation for constant disturbances such as joint friction, utilizing known robot dynamics for increased control performance and compensation for model uncertainties. The disadvantage, however, is that it heavily relies on the performance and robustness of the disturbance observer which is generally limited by the noise associated with sensors. Still, it has been experimentally shown that the proposed control outperforms hybrid velocity/force control with dynamics based PI or conventional PI as the velocity controllers.

The proposed contact normal estimation method is simple such that it only needs an initial value and the tangent force measurements. It is applicable for contour tracking with different kinds of workpieces due to its robustness against discontinuities on the contour, surface roughness, and associated contact friction. It is also flexible such that the parameters K_θ and f_{bias}^t can be selected appropriately for different operations, and for normal force and contour tracking velocity commands.

The presented method has been tested with normal force commands of 10 N and 20 N. It has been seen that having 20 N normal force command does cause jamming of the tooltip at sharp discontinuities while such discontinuities do not pose a problem when the normal force command is 10 N. Testing was also done with contour tracking velocity commands up to 20 mm/s. It has been shown that the contour could be tracked at the experimented velocities but the disturbance observer gains need to be decreased in order to not cause oscillation at higher velocities, which decreases the performance of the control. Given that the system noise is low or mostly removed, the proposed control should handle velocities up to the point where the $\mu(q, \dot{q})$ term of the operational space dynamics equation (2.20) starts to dominate robot dynamics, or up to the point where the delay introduced by low-pass filtering of q causes problems; as long as the acceleration remains at a reasonable level.

4.1. Possible Improvement as Future Work

Adaptive parameter scheduling for contact normal angle estimation: Selection of the learning parameter K_θ depends on the normal force and contour tracking velocity. Moreover, the tangent force bias f_{bias}^t should be selected appropriately for desired operation. A default value for the expected tangent force throughout the contour tracking task needs to be set for satisfactory estimation of the contact direction. An adaptive selection of these parameters according to online measurements can further increase robot autonomy.

Active chatter detection: High disturbance observer gains result in chattering of the estimated disturbance force due to existence of significant system noise. However, when the estimated disturbance is low, the disturbance observer gain may be increased without causing oscillations in order to enable fast reaction to sudden disturbances. Therefore, actively manipulating the disturbance observer gain/bandwidth via chatter detection may be beneficial for the control performance.

REFERENCES

- [1] Murakami, T., Yu, F., & Ohnishi, K. (1993). Torque Sensorless Control in Multidegree-of-Freedom Manipulator. *IEEE Transactions on Industrial Electronics*, 259-265.
- [2] Sariyildiz, E., & Ohnishi, K. (2014). A Guide to Design Disturbance Observer based Motion Control Systems. *International Power Electronics Conference* (pp. 2483-2488). IEEE.
- [3] Coste-Manière, E., Couvignou, P., & Khosla, P. K. (1993). Robotic Contour Following based on Visual Servoing. *IEEE/RSJ International Conference on Intelligent Robots and Systems* (pp. 716-722). Yokohama: IEEE.
- [4] Huang, S., Bergström, N., Yamakawa, Y., Senoo, T., & Ishikawa, M. (2016). High-Performance Robotic Contour Tracking based on Dynamic Compensation Concept. *IEEE International Conference on Robotics and Automation* (pp. 3886-3893). Stockholm: IEEE.
- [5] Shaheen, A., & Lee, C. N. (1990). Shape Recovery from Robot Contour-Tracking with Force Feedback. *IEEE International Conference on Robotics and Automation* (pp. 447-452). Cincinnati: IEEE.
- [6] Raibert, M. H., & Craig, J. J. (1981). Hybrid Position/Force Control of Manipulators. *Journal of Dynamics Systems, Measurement, and Control*, 126-133.
- [7] Yoshikawa, T., & Sudou, A. (1993). Dynamic Hybrid Position/Force Control of Robot Manipulators - On-Line Estimation of Unknown Constraint. *IEEE Transactions on Robotics and Automation*, 220-226.
- [8] Bossert, D., Uy-Loi, L., & Vagners, J. (1996). Experimental Evaluation of a Hybrid Position and Force Surface Following Algorithm for Unknown Surfaces. *IEEE International Conference on Robotics and Automation* (pp. 2252-2257). Minneapolis: IEEE.
- [9] Whitcomb, L. L., Arimoto, S., Naniwa, T., & Ozaki, F. (1997). Adaptive Model-Based Hybrid Control of Geometrically Constrained Robot Arms. *IEEE Transactions on Robotics and Automation*, 105-116.
- [10] Jatta, F., Adamini, R., Visioli, A., & Legnani, G. (2002). Hybrid Force/Velocity Robot Contour Tracking: an Experimental Analysis of Friction Compensation Strategies. *IEEE International Conference on Robotics and Automation* (pp. 1723-1728). Washington DC: IEEE.
- [11] Jatta, F., Legnani, G., & Visioli, A. (2006). Friction Compensation in Hybrid Force/Velocity Control of Industrial Manipulators. *IEEE Transactions on Industrial Electronics*, 604-612.

- [12] Mi, L., & Yan-Bin, J. (2004). High Precision Contour Tracking with a Joystick Sensor. *IEEE/RSJ International Conference on Intelligent Robots and Systems* (pp. 804-209). Sendai: IEEE.
- [13] Ohnishi, K., Shibata, M., & Murakami, T. (1996). Motion Control for Advanced Mechatronics. *IEEE/ASME Transactions on Mechatronics*, 56-67.
- [14] Kobayashi, H., Katsura, S., & Ohnishi, K. (2007). An Analysis of Parameter Variations of Disturbance Observer for Motion Control. *IEEE Transactions on Industrial Electronics*, 3413-3421.
- [15] Sariyildiz, E., & Ohnishi, K. (2014). A Guide to Design Disturbance Observer. *Journal of Dynamics Systems, Measurement, and Control*, 021011-1 - 021011-10.
- [16] Sabanovic, A., & Ohnishi, K. (2011). *Motion Control Systems*. John Wiley & Sons (Asia) Pte Ltd.
- [17] Spong, M. W., Hutchinson, S., & Vidyasagar, M. (2006). *Robot Modeling and Control*. John Wiley & Sons, Inc.